MNRAS 000, 1–20 (2018) Preprint 7 April 2024 Compiled using MNRAS LATEX style file v3.0

A radial velocity survey of the Carina Nebula's O-type stars

Megan M. Kiminki[1]★ and Nathan Smith[1]
[1]Steward Observatory, University of Arizona, 933 N. Cherry Avenue, Tucson, AZ 85721, USA

Accepted 2018 March 14. Received 2018 March 11; in original form 2017 June 17.

ABSTRACT

We have obtained multi-epoch observations of 31 O-type stars in the Carina Nebula using the CHIRON spectrograph on the CTIO/SMARTS 1.5-m telescope. We measure their radial velocities to 1–2 km s^{-1} precision and present new or updated orbital solutions for the binary systems HD 92607, HD 93576, HDE 303312, and HDE 305536. We also compile radial velocities from the literature for 32 additional O-type and evolved massive stars in the region. The combined data set shows a mean heliocentric radial velocity of 0.6 km s^{-1}. We calculate a velocity dispersion of $\leq$ 9.1 km s^{-1}, consistent with an unbound, substructured OB association. The Tr 14 cluster shows a marginally significant 5 km s^{-1} radial velocity offset from its neighbor Tr 16, but there are otherwise no correlations between stellar position and velocity. The O-type stars in Cr 228 and the South Pillars region have a lower velocity dispersion than the region as a whole, supporting a model of distributed massive-star formation rather than migration from the central clusters. We compare our stellar velocities to the Carina Nebula's molecular gas and find that Tr 14 shows a close kinematic association with the Northern Cloud. In contrast, Tr 16 has accelerated the Southern Cloud by 10–15 km s^{-1}, possibly triggering further massive-star formation. The expansion of the surrounding H II region is not symmetric about the O-type stars in radial velocity space, indicating that the ionized gas is constrained by denser material on the far side.

Key words: binaries: spectroscopic – ISM: evolution – open clusters and associations: individual: Carina Nebula – stars: early-type – stars: kinematics and dynamics – stars: massive

1 INTRODUCTION

The Carina Nebula is one of the most dramatic star-forming regions in the nearby Galaxy. It is home to more than 70 O-type stars (Smith 2006; Gagné et al. 2011; Alexander et al. 2016), including the defining star of the O2 spectral type (Walborn et al. 2002a), as well as three late-type hydrogen-rich Wolf-Rayet stars (WNH stars; Smith & Conti 2008) and the remarkable luminous blue variable η Carinae (Davidson & Humphreys 1997). The distribution of these O-type and evolved massive stars is shown in Figure 1. Roughly half belong to two central clusters, Trumpler (Tr) 14 and Tr 16, while the rest are spread across an area more than 30 pc in diameter. Most of the more distributed stellar population is found in the South Pillars, a region of active star formation to the south of Tr 16 (Smith et al. 2000, 2010b). The combined ionizing radiation and stellar winds from the clustered and distributed massive stars (Smith & Brooks 2007) has had a major impact on their surroundings, shaping spectacular dust pillars (Smith et al. 2000, 2010b), powering a developing superbubble (Smith et al. 2000), and potentially triggering the observed ongoing star formation (Megeath et al. 1996; Smith et al. 2000; Rathborne et al. 2004; Smith et al. 2005, 2010b). The feedback-dominated environment of the Carina Nebula is the closest analogue to giant starburst regions like 30 Doradus (e.g., Doran et al. 2013).

Due to the physical extent and complex structure of the Carina Nebula, the relationships between its various clusters and subclusters have been the subject of considerable debate. Photometric and spectroscopic surveys of the stellar populations of Tr 14 and Tr 16 have usually placed the two clusters at a common distance in the range 2.0 to 3.5 kpc (Feinstein et al. 1973; Walborn 1982a,b; The et al. 1980a,b; Turner & Moffat 1980; Tapia et al. 1988; Cudworth et al. 1993; Massey & Johnson 1993; Tovmassian et al. 1994; Tapia et al. 2003; Hur et al. 2012). Other studies concluded that Tr 14 lies 1–2 kpc behind Tr 16 (Walborn 1973; Morrell et al. 1988) or vice versa (Carraro et al. 2004). The smaller Tr 15 cluster likewise alternated between being considered a foreground (Thé & Vleeming 1971) or background (Walborn 1973) cluster, until recent X-ray data revealed a stellar bridge between Tr 15 and Tr 14 (Feigelson et al. 2011). The open cluster Collinder (Cr) 228 and the distributed massive stars of the South Pillars region have been variously treated as an extension of Tr 16 (Walborn 1995; Smith & Brooks 2008), a distinct but same-distance cluster (Herbst 1976; Turner & Moffat 1980; Tapia et al. 1988; Tovmassian et al. 1994; Massey et al. 2001, and see also Smith et al. 2010b and Feigelson et al. 2011), or a foreground cluster (Feinstein et al. 1976; Forte 1978; Carraro & Patat 2001). The optical studies were complicated by the variable ex-

★ E-mail: mbagley@email.arizona.edu

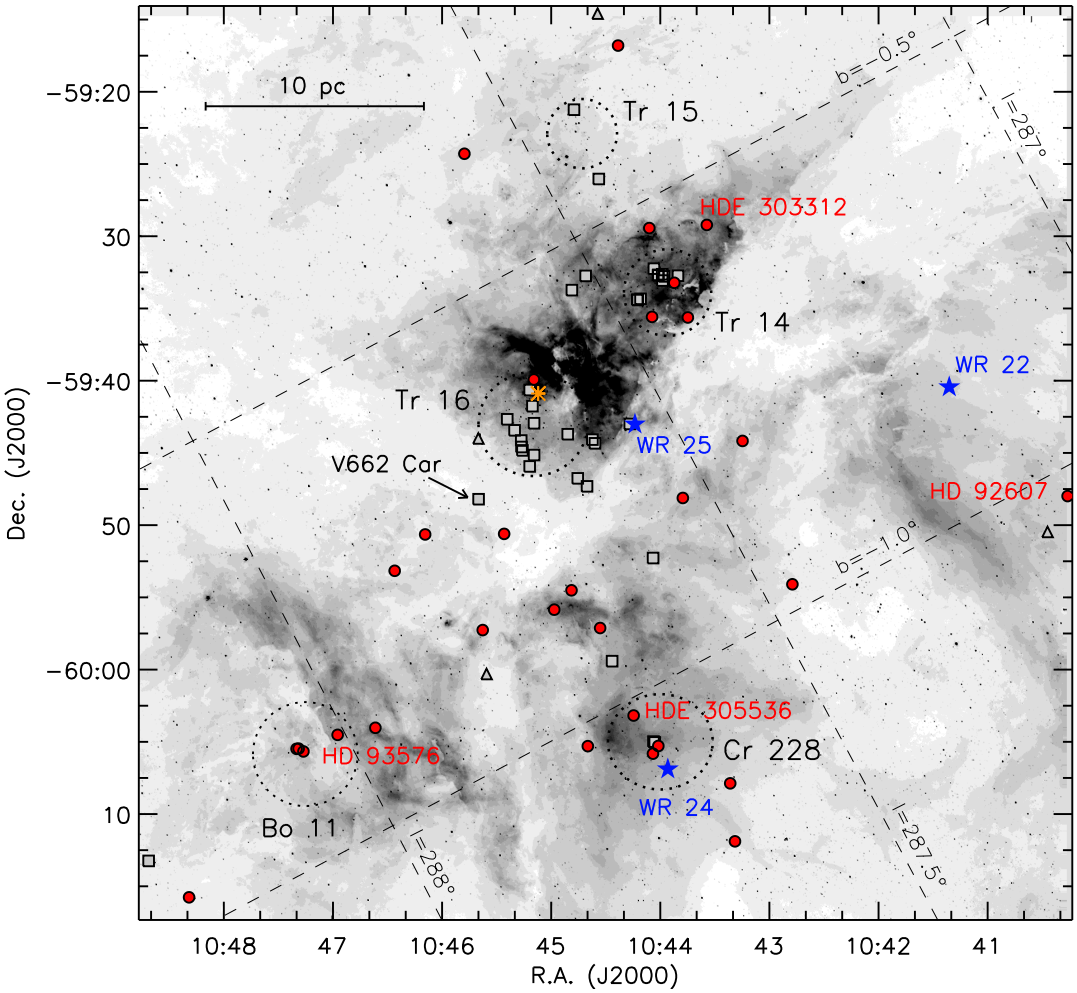

Figure 1. The O-type and evolved massive stars in the Carina Nebula, shown over a ground-based Hα image from Smith et al. (2010a) with Galactic coordinates overlaid for reference. Red circles are O-type stars with new CHIRON observations; we identify by name the four spectroscopic binaries with new orbital solutions (see Section 3). Gray squares are O-type stars in version 3.1 of the Galactic O-Star Catalog (Maíz Apellániz et al. 2013; Sota et al. 2014) that were not targeted with CHIRON. The V662 Car system (see Section 4.3.2) is highlighted. Gray triangles are additional O-type stars confirmed by Alexander et al. (2016). The three WNH stars are marked with blue stars, and η Car is indicated by an orange asterisk. The large dashed circles mark the approximate locations of the major clusters in the region.

tinction across the region and the unusually high ratio of total-to-selective extinction R_V (Herbst 1976; Forte 1978; The et al. 1980a,b; Smith 1987; Tovmassian et al. 1994; Carraro et al. 2004; Mohr-Smith et al. 2017).

Independent of the many spectrophotometric distance studies of the region, measurements of the expansion of η Car's Homunculus Nebula have placed that star at a firm distance of 2.3 kpc (Allen & Hillier 1993; Davidson et al. 2001; Smith 2006). As there is strong evidence that η Car is a member of Tr 16 (Walborn & Liller 1977; Allen 1979) and gas pillars across the Carina Nebula complex show the influence of Tr 16's feedback (Smith et al. 2000, 2010b), a general consensus has arisen that Tr 14, Tr 16, Cr 228, and the rest of the stars in the Carina Nebula belong to a single massive association at 2.3 kpc (e.g., Smith & Brooks 2008, although see Hur et al. 2012). Preliminary results from *Gaia* Data Release 1 (DR1; Gaia Collaboration et al. 2016a,b; Lindegren et al. 2016), which includes 43 of the Carina Nebula's O-type stars, support this interpretation. The inferred parallax-based distances, as computed by Astraatmadja & Bailer-Jones (2016) using a prior based on the distribution of stars in the Milky Way, are distributed unimodally around ~ 2 kpc (Smith & Stassun 2017).

Even with the spatial link between the Carina Nebula's components now relatively secure, the formation of its distributed massive population remains somewhat uncertain. The O-type stars currently seen among the South Pillars may have been born there, a possible example of an OB association forming through distributed, hierarchical star formation (e.g., Efremov & Elmegreen 1998; Clark et al. 2005). But no massive protostars have been detected among the forming stellar population in the South Pillars (Gaczkowski et al. 2013), and Preibisch et al. (2011) argue that the dense gas clouds in the region are not massive enough to support further massive-star formation. If the distributed O-type stars did not form in situ, they may have migrated out from Tr 16 either through the classic expansion of a cluster after gas dispersal (Tutukov 1978; Hills 1980; Lada & Lada 1991, 2003) or as the result of cluster-cluster interaction (Gieles 2013) between Tr 14 and Tr 16. Kiminki et al. (2017) did not see any such outward migration in the local proper motions of bow-shock-associated massive stars in the South Pillars, but their sample size was limited.

In this paper, we explore the relationships between the components of the Carina Nebula and the origins of its massive-star populations through a survey of the radial velocities (RVs) of its O-type and evolved massive stars. These stellar RVs can be compared to the kinematics of the Carina Nebula's H II regions (e.g., Damiani et al. 2016) and molecular gas (e.g., Rebolledo et al. 2016), allowing a direct assessment of the impact of massive-star feedback on the interstellar medium. The RVs of massive stars can be strongly affected by stellar binarity (e.g., Gieles et al. 2010), but the effects can be constrained with multi-epoch observations.

The paper is organized as follows: In Section 2, we describe our multi-epoch spectroscopic observing campaign and our RV measurements, and summarize the additional data compiled from the literature. In Section 3, we discuss the O-type stars with variable RVs and present orbital solutions for four spectroscopic binary systems. Section 4 discusses the RV distributions of the various O-star populations in the Carina Nebula and compares the observed stellar kinematics to the motions of the region's molecular and ionized gas. Our conclusions are summarized in Section 5. Projected distances between sources are given using the η Car distance of 2.3 kpc.

2 OBSERVATIONS AND DATA ANALYSIS

2.1 Target selection

Our list of O-type stars in the Carina Nebula is drawn from version 3.1 of the Galactic O-Star Catalog (GOSC; Maíz Apellániz et al. 2013; Sota et al. 2014). The GOSC v3.1 lists 68 objects, including the Of/WNH system WR 25, with right ascensions between 10:40:00 and 10:49:00 and declinations between −60:20:00 and −59:10:00. An additional four O-type systems in this coordinate range, originally suspected on the basis of their X-ray emission (Povich et al. 2011b), were recently spectroscopically confirmed by Alexander et al. (2016). Adding η Car and the remaining two WNH stars brings the total number of known systems with O-type and evolved massive primaries to 75. These 75 systems are shown in Figure 1.

We selected 31 of these systems for new spectroscopic observations. In choosing targets, we prioritized stars that had zero or few prior RV measurements, or whose only existing RV data had high uncertainties. Most of our target stars are thus outside of Tr 14 and Tr 16, as those clusters have been the targets of multiple spectroscopic campaigns and binary fraction analyses (Penny et al. 1993; García et al. 1998; Albacete Colombo et al. 2001, 2002; Morrell et al. 2001; Rauw et al. 2001, 2009; Nazé et al. 2005; Niemela et al. 2006). We also prioritized sources brighter than $V = 11$ mag.

2.2 Spectroscopy

We obtained high-resolution spectra of our 31 target stars with the CHIRON echelle spectrograph (Tokovinin et al. 2013) on the CTIO 1.5-m telescope operated by the SMARTS Consortium. Observations were taken in queue operation using the fiber mode configuration, which provides a resolution of R ∼25,000 over a wavelength range of 4100–8900 Å. All 31 stars were observed 2–4 times each in Nov–Dec 2014. Observations of a given star were spaced 7–14 days apart to minimize the chances of catching a short-period binary at the same phase, as there is a relative lack of massive binaries in this period range (Kiminki & Kobulnicky 2012; Kobulnicky et al. 2014). Follow-up observations of eight stars showing possible RV variations were obtained in Oct 2015–Jan 2016. Throughout our observing campaign, exposure times were 60–1800 s, designed to achieve signal-to-noise (S/N) ratios of 50–70 at 5500 Å. The resulting S/N ratios ranged from 30 to 150 with a median of 77. ThAr calibration spectra were taken before moving the telescope after observing each star; bias and flat-field observations were taken at the beginning and end of each night as part of CHIRON's standard queue observing protocol.

Data were reduced in `IRAF`[1] using standard procedures, including bias subtraction, flat-fielding, cosmic ray correction, and extraction of 74 echelle orders. Wavelength calibration was performed using the corresponding ThAr spectrum for each star, and wavelengths were corrected to a heliocentric frame. The wavelength scale of each order is good to an rms of 0.01 Å (∼0.6 km s^{-1} at 5000 Å). Echelle orders were continuum-normalized before being combined into a single spectrum for each exposure. A representative sample of reduced spectra is shown in Figure 2, focusing on a wavelength region that covers most of the lines used for RV measurement (see Section 2.3).

2.3 New radial velocities

We adapt the method of Sana et al. (2013) for measuring stellar RVs, performing Gaussian fits to a set of He lines and fitting all lines and epochs for a given star simultaneously. The final fit forces all lines at a given epoch to have the same RV, and assumes that the width and amplitude of a given spectral line are constant across epochs. The uncertainties on initial, single-line fits are used to weight each line in the final overall fit. We use the IDL curve-fitting package `MPFIT` (Markwardt 2009).

Like Sana et al. (2013), we fit to the He absorption lines for two reasons. First, these lines are present across all O subtypes (unlike most metal lines), allowing us to apply a consistent approach to our full sample of observed stars. Second, the He lines are relatively less sensitive to wind effects compared to the hydrogen Balmer series (Bohannan & Garmany 1978; see also discussion in Sana et al. 2013). Initially, we fit He I $\lambda\lambda$4387, 4471, 4713, 4922, 5015, 5876, 6678, 7065 and He II $\lambda\lambda$4541, 4686. The rest wavelengths adopted for these lines are given in Table 1. After the first round of fits, we compared the RVs from individual line fits to the RVs from fitting all lines at once. The triplet blend He I λ4471 was systematically blueshifted by ∼10 km s^{-1} relative to the overall results, and the singlet line He I λ6678 was systematically redshifted by a similar amount. We therefore removed those two lines and refit all epochs of the observed stars. We did not see a systematic offset in the RVs of He II λ4686, likely because the majority of our targets are mid- to late-type main-sequence O stars, in which this line is not strongly affected by winds (Sana et al. 2013). Wind emission in He II λ4686 is apparent in the spectra of the supergiant HD 93632 (see Figure 2), and we excluded this line in that star's final fit. On a star-by-star basis, we also excluded other lines that were affected by emission from stellar winds or from the surrounding H II region, as well as lines that were not present above the noise level of the continuum. With these exclusions, an average of seven absorption lines were used to fit the RVs of each star. The measured RVs for each star at

[1] `IRAF` is distributed by the National Optical Astronomy Observatory, which is operated by the Association of Universities for Research in Astronomy (AURA) under a cooperative agreement with the National Science Foundation.

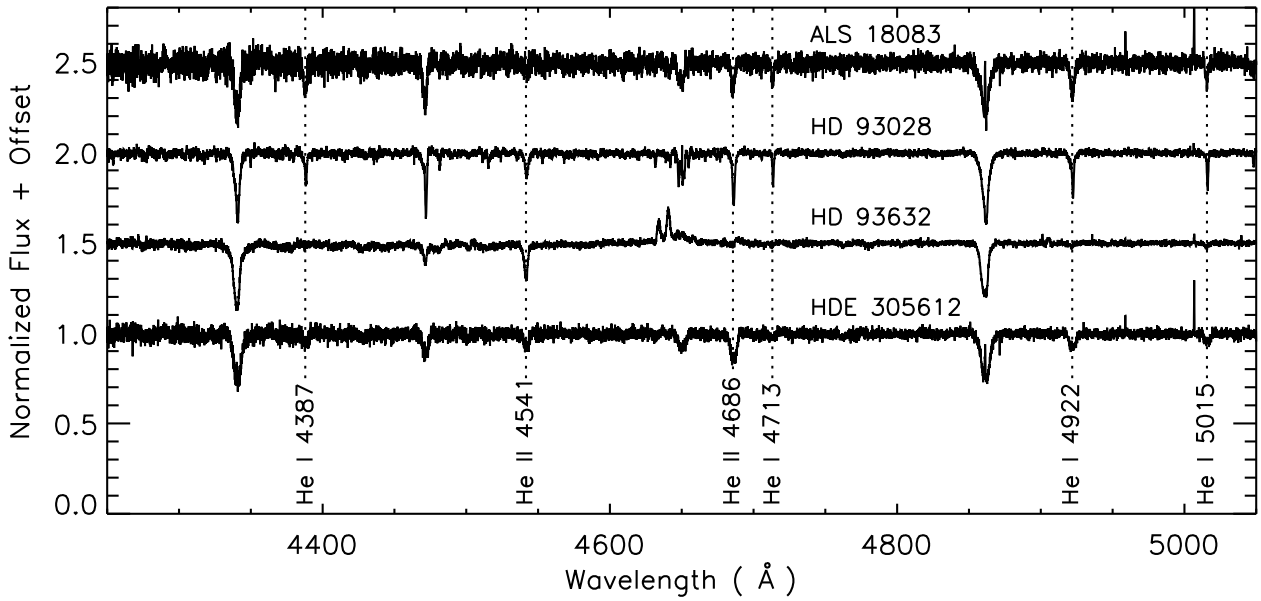

Figure 2. Continuum-normalized CHIRON spectra of four O-type stars in our observed sample, illustrating the range of S/N achieved in the wavelength range 4250–5050 Å. Stellar radial velocities were measured using fits to the marked He I and He II absorption lines and He I $\lambda\lambda$5876, 7065, where present without emission components.

Table 1. Rest wavelengths used to compute radial velocities.

Line	Wavelength (Å)	Reference[a]
He I λ4387	4387.9296	NIST
He I λ4471[b]	4471.4802	NIST
He II λ4541	4541.591	PvH
He II λ4686	4685.71	PvH
He I λ4713	4713.1457	NIST
He I λ4922	4921.9313	NIST
He I λ5015	5015.6783	NIST
He I λ5876	5875.621	NIST
He I λ6678[b]	6678.151	NIST
He I λ7065	7065.190	NIST

[a]NIST = NIST Atomic Spectra Database (Kramida et al. 2016); PvH = Peter van Hoof's Atomic Line List, v2.04 (http://www.pa.uky.edu/~peter/atomic/).
[b]Excluded from final fits.

Table 2. Heliocentric radial velocities measured from CHIRON observations of O-type stars in the Carina Nebula. Dates are given for the midpoints of the exposures. This table is available in its entirety as Supplementary Material to the online version of this article. A portion is shown here for guidance regarding its form and content.

Name	HJD −2400000	RV1 (km s^{-1})	σ(RV1) (km s^{-1})	RV2 (km s^{-1})	σ(RV2) (km s^{-1})
ALS 15204	56987.814	-60.0	4.7	...	...
ALS 15204	56994.850	1.0	2.3	...	...
ALS 15204	57003.836	43.1	2.0	...	...
ALS 15206	56992.858	24.5	0.4	...	...
ALS 15206	57000.851	29.8	0.5	...	...
ALS 15206	57008.788	34.1	0.3	...	...

each epoch are given in Table 2. The median uncertainty in RV for the single-lined spectra is 1.2 km s^{-1}.

One of our observed sources, HD 92607, is a double-lined spectroscopic binary (SB2), first identified by Sexton et al. (2015). We adapted our RV measurement procedure to fit a double Gaussian at all epochs. This process required several steps: First, we fit He I λ5876 for the six epochs in which the components were clearly separated. Then, we fixed the width and amplitude of the He I λ5876 components and fit to the four epochs with blended components. These fits gave us initial estimates for the RVs at all epochs, which we used as the starting point for fits to He I $\lambda\lambda$4922, 5015 and He II λ4686. Again, we fit these lines in the well-separated epochs first, then fixed widths and amplitudes for fits to the blended epochs. The final fit was to all four lines at all epochs. Because the two components of HD 92607 are of similar spectral type, several iterations of line fitting and orbital analysis (see Section 3.1) were required to confidently identify which line component was associated with which star at a given epoch. The median uncertainty on the RVs of the components of HD 92607 is 7.1 km s^{-1}, and ranges as high as 30–40 km s^{-1} in epochs where the lines are highly blended.

As a check on our wavelength calibration, we obtained CHIRON spectra of the RV standard stars HIP 51722 (spectral type F7–8 V) and HIP 53719 (K1–2 IV), both from the catalog of Soubiran et al. (2013), in Nov 2014. As the spectra of these standard stars do not have He I lines, their RVs could not be measured by the same method used for our science spectra. Instead, we measured their RVs by cross-correlation with high-resolution stellar spectra from Coelho (2014), using the `IRAF` task `fxcor`. The measured RVs of both standard stars agree with their expected values within 0.4 km s^{-1}.

2.4 Radial velocities from the literature

Where available, we also compiled heliocentric RVs from the literature for the Carina Nebula's O-type and evolved massive stars. The adopted RVs and associated uncertainties for stars not observed with CHIRON are given in Table 3 along with the corresponding references. Nearly all of these RVs were measured from various subsets of He absorption lines, often in conjunction with metal and/or hydrogen Balmer lines. The exceptions are: η Car, where the systemic radial velocity was derived from H_2 emission from the Homunculus (Smith 2004); the three WNH stars, discussed further below; and the Conti et al. (1979) RVs for the Of supergiant HD 93129A, where we use RVs from the "Group 1" narrow metal lines. Where a system is a spectroscopic binary with a published orbital solution, we give the systemic velocity; for other sources with observations at multiple epochs, we give the weighted mean of the available velocities. For visual binaries that are resolvable at the few-arcsecond level (e.g., HD 93161AB), we use only data that specify which component was observed. We also note whether systems were classified as constant-RV or binary in the multiplicity survey of Chini et al. (2012). Additional notes on the spectroscopic multiplicity of a system are given in the references column. We also incorporate literature data for the following CHIRON targets: ALS 15206 (Huang & Gies 2006), ALS 15207 (García et al. 1998), HD 93028 (Feast et al. 1957; Conti et al. 1977), HDE 303308 (Conti et al. 1977), HDE 305518 (Huang & Gies 2006), and HDE 305619 (Humphreys 1973). In no case does the inclusion of these sources' literature RVs shift their overall weighted mean RV by more than 1.5 km s^{-1}.

As mentioned above, the three WNH stars are a special case. Like all Wolf-Rayet stars, these sources have strong stellar winds, with their spectral features formed at various depths within those winds (e.g., Crowther 2007). Consequently, the observed RVs vary greatly depending on which lines are measured. Relative to the stars' systemic velocities, the hydrogen Balmer and He II absorption lines of Wolf-Rayet spectra tend to be highly blueshifted (Moffat 1978; Moffat & Seggewiss 1978; Conti et al. 1979; Massey & Conti 1981; Rauw et al. 1996), while their He II emission lines tend to be highly redshifted (Moffat 1978; Moffat & Seggewiss 1978; Massey 1980; Niemela & Moffat 1982; Schweickhardt et al. 1999; Schnurr et al. 2008). In WN and WNH spectra, certain narrow N III, N IV, and Si IV emission lines are thought to be relatively better tracers of the true stellar RVs (e.g., Moffat 1978; Moffat & Seggewiss 1978, 1979; Conti et al. 1979). For the Carina Nebula's WNH stars, we adopt RVs measured from N IV λ4058 emission.

However, it is clear that the adopted RVs for the WNH stars are still affected by winds. Using the spectral features of the O-type companion to WR 22, Rauw et al. (1996) calculated the true systemic velocity of the binary to be 21.3 ± 7.0 km s^{-1}, while Schweickhardt et al. (1999) report ≈ 0 ± 15 km s^{-1} for the same source. The N IV λ4058 line in the spectrum of WR 22 is thus blueshifted by ∼ 25–50 km s^{-1}. In other WN+O binaries, this line shows relative blueshifts of 0–80 km s^{-1} (Niemela et al. 1980; Niemela & Moffat 1982; Collado et al. 2013, 2015; Munoz et al. 2017). Because the exact magnitude of the shift is uncertain and seems to vary by star, we do not attempt to correct the N IV λ4058 RVs for wind effects, and we consider the three WNH stars as a separate group in our analysis. Note that although η Car is also an evolved massive star with a high mass-loss rate, its RV was measured by a different method (Smith 2004) and it does not suffer from the same bias.

In compiling literature RVs for Table 3, we found that the RVs in Levato et al. (1990, 1991a,b) are notably discrepant with later observations, including our own. These three studies measured RVs from an unspecified subset of hydrogen Balmer and He absorption lines for a total of 92 candidate members of Cr 228, Tr 16, and Tr 14, using the spectrograph on the 1-m Yale CTIO telescope (see Levato et al. 1986). They computed average cluster RVs of −23, −26, and −29 km s^{-1} for Cr 228, Tr 16, and Tr 14, respectively. By contrast, the surveys of Penny et al. (1993) and García et al. (1998) found +2.8 km s^{-1} and +6.0 km s^{-1}, respectively, for the average RV of Tr 14. Penny et al. (1993) also reported very different results from Levato et al. (1991b), in both RV values and variability, for individual sources in Tr 14. Across the Carina Nebula, we find that the Levato et al. (1990, 1991a,b) data are typically 10–60 km s^{-1} more negative than other literature values for the same stars (see Table 3) and our CHIRON observations. We therefore exclude all data from the Levato et al. studies, except for specific binary orbits as discussed in Section 3.

With the inclusion of the literature data in Table 3, we have RVs for 63 of the 75 O-type and evolved massive stars in the Carina Nebula. Four of the twelve stars without RV data are those that were newly confirmed by Alexander et al. (2016). These four are relatively highly extincted, with a median A_V of 5.7 mag compared to the median A_V of 2.2 mag for the rest of the O-type stars in the region (Gagné et al. 2011; Povich et al. 2011a). Alexander et al. (2016) postulate that one of these, OBc 3, is a coincidentally aligned background star. The other eight stars without RV data are neither systematically more extincted nor systematically fainter at visual wavelengths than the 63 sources with RV data. Some of these eight have been observed as part of the OWN RV survey (Barbá et al. 2010; see Sota et al. 2014; Maíz Apellániz et al. 2016) but currently lack published RVs.

3 NEW AND UPDATED BINARY ORBITS

Multiplicity is ubiquitous among O-type stars (Garmany et al. 1980; Mason et al. 2009; Chini et al. 2012; Sana et al. 2012, 2013, 2014; Kobulnicky et al. 2014; Moe & Di Stefano 2017) and must be considered when determining their systemic RVs. For each of our CHIRON sources, we compute $P(\chi^2, \nu)$, the probability that the χ^2 about the weighted mean would be exceeded by random chance given $\nu = N_{\rm obs} - 1$ degrees of freedom. Nine of the 31 observed stars display significant ($P(\chi^2, \nu) < 0.01$) RV variations with amplitudes > 20 km s^{-1} in our CHIRON data. As discussed below, we are able to find periods and fit orbital solutions to four of these spectroscopic binaries. Two additional observed sources meet the criteria for significant, high-amplitude variations when their literature RVs are included. One of these sources is HD 93403, a known SB2 with a full orbital solution in Rauw et al. (2000). Our CHIRON observations are in good agreement with the orbit of the primary star, and we adopt the systemic velocity for HD 93403 from the Rauw et al. (2000) solution.

An additional five CHIRON targets display significant ($P(\chi^2, \nu) < 0.01$) but low-amplitude (ΔRV < 20 km s^{-1}) RV variations. These stars include HDE 305619, which was flagged as an SB1 by Chini et al. (2012) but lacks published RV data. The other four stars may have undetected long-period companions or may be showing photospheric variability (e.g., Garmany et al. 1980; Gies & Bolton 1986; Fullerton et al. 1996; Ritchie et al. 2009; Martins et al. 2015).

We search for orbital solutions for the stars with significant,

Table 3. Mean or systemic heliocentric radial velocities adopted from the literature.

Name	$\overline{RV}$ or γ (km s^{-1})	$\sigma(\overline{RV})$ (km s^{-1})	Spectral flag from Chini et al. (2012)[a]	References
ALS 15229	14.7	3.5	...	García et al. (1998)
CPD-58 2611	4.7	5.0	C[b]	Penny et al. (1993); García et al. (1998)
CPD-58 2620	-0.6	5.8	SB1	Penny et al. (1993); García et al. (1998)
CPD-59 2591	-2.9	10.	...	Huang & Gies (2006)
CPD-59 2624	13.5	10.	...	Huang & Gies (2006); SB2 in Alexander et al. (2016)
CPD-59 2626	-22.7	10.	...	Huang & Gies (2006)
CPD-59 2627	-15.9	10.	...	Huang & Gies (2006)
CPD-59 2629	-8.8	12.8	...	SB1 in Williams et al. (2011)
CPD-59 2635	0.	1.	SB2	SB2 solution from Albacete Colombo et al. (2001)
CPD-59 2636	4.0	5.7	SB2	Quadruple system; Albacete Colombo et al. (2002)
CPD-59 2641	-4.5	1.8	SB2	SB2 solution from Rauw et al. (2009)
η Carinae	-8.1	1.	...	Smith (2004)
HD 93128	5.0	5.3	C[b]	Penny et al. (1993); García et al. (1998)
HD 93129A	-10.1	18.7	C[b]	Conti et al. (1979); Penny et al. (1993)
HD 93129B	7.1	2.2	...	Penny et al. (1993)
HD 93160	-12.9	17.9	SB1	Thackeray et al. (1973); Conti et al. (1977)
HD 93161A	1.1	3.6	SB2	SB2 data from Nazé et al. (2005)
HD 93161B	-25.4	28.4	...	Nazé et al. (2005)
HD 93130	59.9	3.1	SB2	Conti et al. (1977)
HD 93204	8.5	3.8	C	Conti et al. (1977)
HD 93205	-2.9	0.9	SB2	SB2 solution from Morrell et al. (2001)
HD 93250	-5.2	7.6	C[b]	Thackeray et al. (1973); Rauw et al. (2009); Williams et al. (2011)
HD 93343	-2.8	54.4	SB2	SB2 data from Rauw et al. (2009)
HD 93403	-14.2	5.4	SB2	SB2 solution from Rauw et al. (2000)
HD 93843	-9.9	0.4	C	Feast et al. (1957); Conti et al. (1977)
QZ Car	-8.7	15.5	SB2	Quadruple system; Morrison & Conti (1980); Mayer et al. (2001)
Trumpler 14-9	5.6	3.8	...	Penny et al. (1993); García et al. (1998)
V572 Car	-3.4	3.7	SB2	Triple system; Rauw et al. (2001)
V573 Car	-5.	4.	...	SB2 solution from Solivella & Niemela (1999)
V662 Car	-15.	2.	...	SB2 solution from Niemela et al. (2006)
WR 22[c]	-27.5	...	...	SB1 solution from Schweickhardt et al. (1999)
WR 24[c]	-34.0	13.3	...	Conti et al. (1979)
WR 25[c]	-34.6	0.5	...	SB1 solution from Gamen et al. (2006)

[a]C = constant; SB1 = single-lined spectroscopic binary; SB2 = double-lined spectroscopic binary.
[b]Although classified as constant in Chini et al. (2012), these stars meet our criteria for significant RV variability ($P(\chi^2, \nu) < 0.01$; see Section 3) and have RV amplitudes > 20 km s^{-1}.
[c]Reported RVs are from N IV λ4058 emission; see discussion in Section 2.4.

Table 4. Orbital and physical parameters of new and updated binary solutions.

Element	HD 92607	HD 93576	HDE 303312	HDE 305536
P (d)	3.6993 (0.0001)	1.852102 (0.000002)	9.4111 (fixed)	1.88535 (0.00002)
e	0.00 (fixed)	0.075 (0.009)	0.58 (fixed)	0.129 (0.008)
γ (km s^{-1})	8.8 (1.6)	-8.4 (0.6)	2.3 (0.6)	2.3 (0.2)
ω (°)	90 (fixed)	201 (9)	192 (2)	56 (3)
T_p (HJD−2400000)	56965.910 (0.009)	57005.94 (0.05)	56980.58 (0.03)	56975.34 (0.02)
K_1 (km s^{-1})	224 (3)	85.0 (0.8)	71 (1)	37.3 (0.3)
K_2 (km s^{-1})	242 (3)	...	...	...
$f(M_1, M_2)$ (M$_\odot$)	...	0.117 (0.004)	0.19 (0.01)	0.0099 (0.0004)
$M_1 \sin^3 i$ (M$_\odot$)	20.2 (0.6)	...	...	...
$M_2 \sin^3 i$ (M$_\odot$)	18.7 (0.6)	...	...	...
$a_1 \sin i$ (R$_\odot$)	16.4 (0.2)	3.10 (0.03)	10.7 (0.2)	1.38 (0.01)
$a_2 \sin i$ (R$_\odot$)	17.7 (0.2)	...	...	...
rms$_1$ (km s^{-1})	19.7	10.9	5.6	2.8
rms$_2$ (km s^{-1})	23.7	...	...	...

One-sigma uncertainties for each quantity are listed in parentheses.

high-amplitude RV variations and $N_{obs} \geq 7$ using the IDL package `rvfit` (Iglesias-Marzoa et al. 2015). Spectroscopic binary orbits are defined by the following parameters: P (orbital period), e (eccentricity), γ (systemic velocity), ω (argument of periastron), T_p (epoch of periastron), K_1 (primary semi-amplitude), and, where applicable, K_2 (secondary semi-amplitude). `rvfit` uses an adaptive simulated annealing method to find the global χ^2 minimum in the six- or seven-dimensional parameter space. Unlike some orbital fitting codes, `rvfit` does not use an initial estimate of the period. In four cases, described in further detail below, `rvfit` converged on orbital solutions with well-fit phase-folded velocity curves. Parameter uncertainties were computed using `rvfit`'s Markov Chain Monte Carlo (MCMC) algorithm (Iglesias-Marzoa et al. 2015) with 10^5 points. The MCMC provides the probability distribution of each parameter marginalized over all other parameters. For our data, these marginalized histograms are well approximated by Gaussian distributions and we take their standard deviations as the one-sigma uncertainties on the orbital parameters.

During our initial analysis of the variable-RV sources, we computed the frequency power spectrum of each source using A. W. Fullerton's IDL implementation of the one-dimensional `CLEAN` algorithm (Roberts et al. 1987). We confirm the periods returned by `rvfit` by checking against these periodograms, which are presented in Appendix A.

3.1 HD 92607

HD 92607 was first noted as an SB2 by Sexton et al. (2015), who classified its components as O8.5 V + O9 V. It is on the far western side of the Carina Nebula, approximately 25 pc from Tr 14 and 16 (see Figure 1). The lower-mass stellar population in this area, by the edge of the Carina Nebula's northern molecular cloud, is relatively young (< 1 Myr; Kumar et al. 2014). HD 92607 is associated with an extended arc of 24 μm emission, suggestive of a stellar wind bow shock, that points to the southeast (Sexton et al. 2015).

We obtained 12 CHIRON spectra of HD 92607 in 2014–2015. As described in Section 2.3, we adapted our RV-fitting procedure to fit two Gaussian profiles to He I $\lambda\lambda$4922, 5015, 5876 and He II λ4686 across all 12 epochs, using fits to the well-separated epochs to fix the widths and amplitudes of the lines. We used `rvfit` to fit an orbit to the primary and secondary RVs simultaneously. We fit a common apparent systemic velocity to both components.[2]

The best-fitting period for HD 92607 is 3.6993 ± 0.0001 d. Figure 3 shows the progression of He I λ5876 over this period. After our initial orbital fit converged on an eccentricity of zero, we fixed $e = 0$ for further fitting, allowing `rvfit` to treat ω and T_p (which are ill-defined at very low eccentricities) in a consistent manner (see Iglesias-Marzoa et al. 2015). The final best-fitting orbital solution is shown in Figure 4, and the orbital parameters are listed in Table 4. In the best-fitting orbit, the minimum masses of the primary and secondary stars are $M_1 \sin^3 i = 20.2 \pm 0.6$ M$_\odot$ and $M_2 \sin^3 i = 18.7 \pm 0.6$ M$_\odot$, respectively, giving a mass ratio of $q = 0.93 \pm 0.04$. But their spectral types of O8.5 V and O9 V (Sexton et al. 2015), according to the "observational" scale of Martins et al. (2005), have somewhat lower expected masses of $M_1 = 18.8$ M$_\odot$ and $M_2 = 17.1$ M$_\odot$. The apparent discrepancy could be the result of the normal uncertainties on spectral-type classification; for instance, Gagné et al. (2011) list HD 92607 as an O8 V star, although they do not account for its spectroscopic binarity. Or perhaps the components of HD 92607 are slightly older, and hence cooler for their masses, than average main-sequence stars of their types. In any case, the HD 92607 system is likely close to edge-on ($i \sim 90°$), as a smaller inclination would imply implausibly large masses for its component stars.

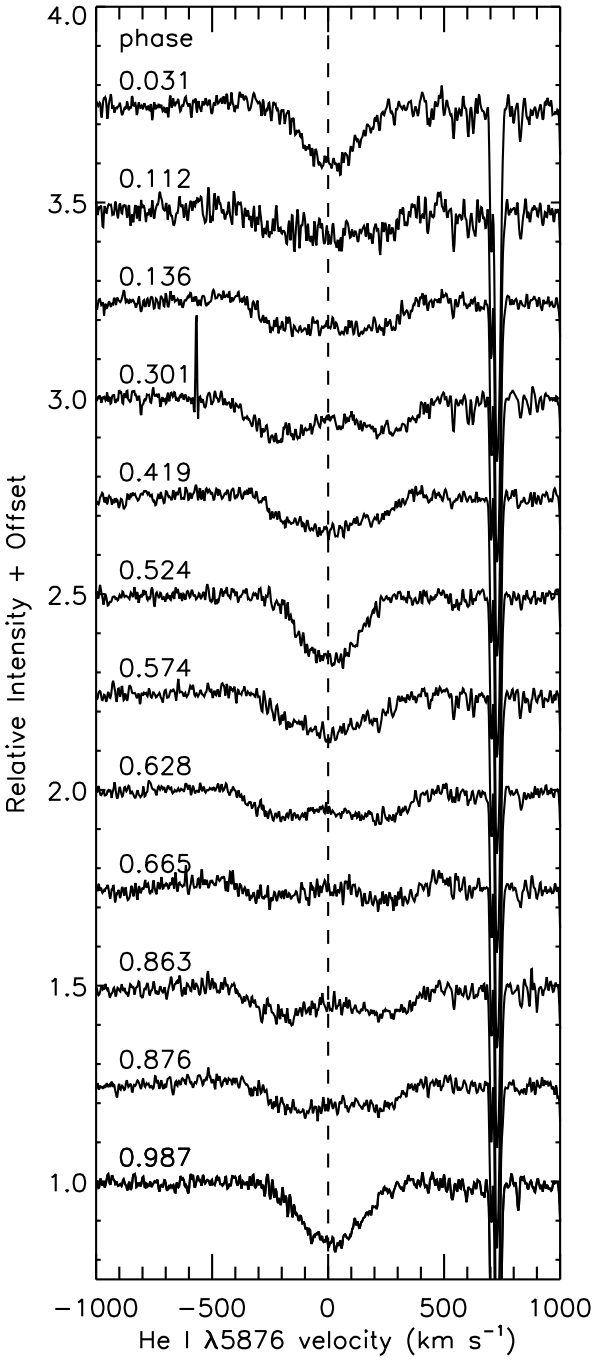

Figure 3. He I λ5876 in velocity space and in order of phase for CHIRON observations of the SB2 HD 92607, for an orbital period of 3.6993 d. The narrow absorption line on the right is interstellar Na I λ5890.

[2] We used an F-test to compare our single-γ solution to the best-fitting orbit computed with different γ values for each component. The latter did not provide a significant improvement in fit ($p = 0.27$).

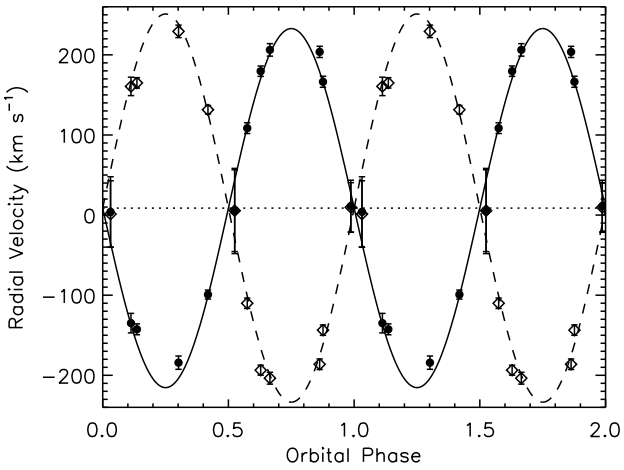

Figure 4. Radial velocity curve and orbital solution for the SB2 HD 92607 at the best-fitting orbital period of 3.6993 d. Filled circles and open diamonds correspond to the primary and secondary components, respectively. The dotted line marks the systemic velocity.

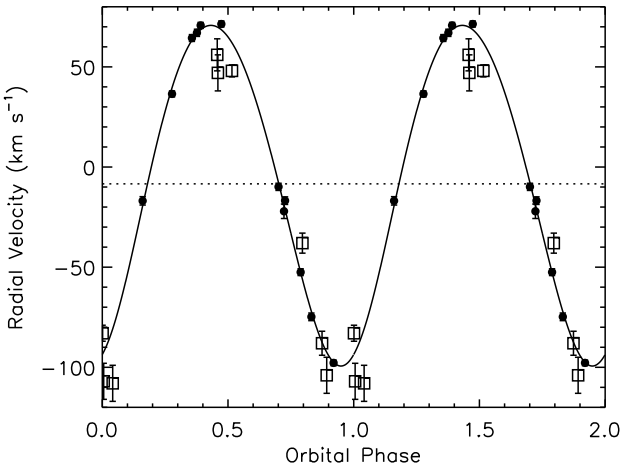

Figure 5. Radial velocity curve and orbital solution for the SB1 HD 93576 at the best-fitting orbital period of 1.852102 d. Solid circles are measurements from our CHIRON spectra and open squares are data from Levato et al. (1990). Both data sets were used to compute the orbital solution. The dotted line marks the systemic velocity.

3.2 HD 93576

HD 93576 is one of five O-type systems in the open cluster Bochum (Bo) 11 in Carina's South Pillars region. Its primary is of type O9–9.5 IV–V (Sota et al. 2014; Sexton et al. 2015). It is associated with an extended arc of 8 μm emission, which points away from Bo 11 and has infrared colors indicative of a stellar wind bow shock (Sexton et al. 2015). Its local proper motion confirms that it is moving away from Bo 11 at $\lesssim$ 15 km s^{-1}; it may have been recently ejected from the cluster (Kiminki et al. 2017).

Levato et al. (1990) first noted periodic RV variations in the spectra of HD 93576, and fit an orbital solution with a period of 2.020 d. We obtained 12 CHIRON observations of this system in 2014–2016. We used `rvfit` to compute orbital solutions both with and without the Levato et al. (1990) data. With our CHIRON data alone, we find a period of 1.85201 d; including the Levato et al. (1990) data constrains the period to 1.852102 ± 0.000002 d. The final best-fitting parameters given in Table 4 and used to plot the orbital solution in Figure 5 are from the combined data set. As can be seen in Figure 5, many but not all of the Levato et al. (1990) RVs for this system are 10–20 km s^{-1} blueshifted relative to CHIRON data at the same phase. Levato et al. (1990) reported a systemic velocity of −21 km s^{-1} for this system, while our fit to the combined data set finds a systemic velocity of −8.4 km s^{-1} and fitting to only our CHIRON data gives a systemic velocity of −8.2 km s^{-1}.

The orbit of HD 93576 is minimally but significantly non-circular, with an eccentricity of 0.075 ± 0.009. The resulting mass function is $f(M_1, M_2) = 0.117 \pm 0.004$ M$_\odot$. Assuming the primary star has a mass of 16–18 M$_\odot$, as appropriate for its spectral type per Martins et al. (2005), the minimum mass of the secondary star is ∼3.7 M$_\odot$, roughly the mass of a B8 V star (Drilling & Landolt 2000).

3.3 HDE 303312

HDE 303312 is an O9.7 IV star (Sota et al. 2014) located on the outskirts of Tr 14 (see Figure 1). There are no RVs for this source in the literature, but it was identified as an eclipsing system by Otero (2006) based on its V-band light curve from the All Sky Automated Survey (ASAS; Pojmanski 1997). Otero (2006) report a period of 9.4109 d and note that it is an "extremely eccentric" system. We obtained a total of 12 CHIRON observations of HDE 303312 over 2014–2015, and downloaded the available ASAS V-band magnitudes for 2000–2009. In addition to using `rvfit` on the velocity data, we use the eclipsing binary modeling programs `PHOEBE` (Prša & Zwitter 2005) and `NIGHTFALL`[3] to synthesize and compare photometric light curves. We find that the ASAS light curve folds most cleanly at a period of 9.4111 d rather than 9.4109 d. We therefore adopt 9.4111 d as the photometric period with an estimated uncertainty of ±0.0002 d.

Initial, unconstrained runs of `rvfit` find an RV period between 9.41 and 9.65 d, with an eccentricity of 0.6–0.7. These results confirm that the eclipsing and spectroscopic binaries are the same system, and we subsequently fix the period at 9.4111 d. With all other orbital parameters left free, the best-fitting solution to the RV data has $e = 0.67$ and $\omega = 188°$. Matching the phase separation of the V-band eclipses for $e = 0.67$ requires $\omega \approx 140°$ or 220°, incompatible with the shape and symmetry of the RV curve. We do not see any shifts in eclipse timing over the nine years of ASAS data that would suggest apsidal motion as an explanation for this discrepancy. We therefore iterate between the the RV curve and light curve to converge on values of e, ω, and inclination i that are consistent with the observed data. Our final best fit to the RV curve, presented in Table 4 and plotted in Figure 6, holds the eccentricity fixed at = 0.58 and gives $\omega = 192 \pm 2°$. The inclination of the system is 80–85°.

This best-fitting orbital solution for HDE 303312 gives a mass function of $f(M_1, M_2) = 0.19 \pm 0.01$ M$_\odot$. If we take the mass of the primary star to be 15–18 M$_\odot$, based on its spectral type (see Martins et al. 2005), the mass of the secondary star is 4–5 M$_\odot$. Assuming the secondary star is on the main sequence, that mass corresponds to a spectral type of B6–7 V (Drilling & Landolt 2000), which would have an effective temperature of $T_{\rm eff} \approx 13,000$–14,000 K (Kenyon & Hartmann 1995). Unfortunately, the noise in the ASAS data prevents us from putting strong constraints on the relative luminosities or stellar radii of the components. High-S/N,

[3] http://www.hs.uni-hamburg.de/DE/Ins/Per/Wichmann/Nightfall

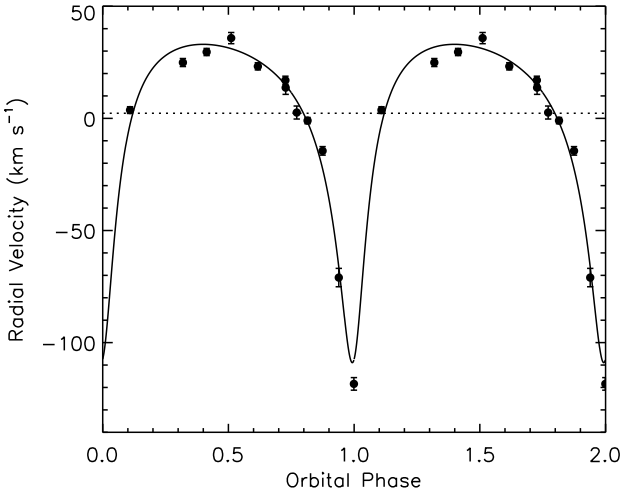

Figure 6. Radial velocity curve and orbital solution for the eclipsing SB1 HDE 303312. The solid line shows the best-fitting orbital solution to the RV data with the period and eccentricity fixed at 9.4111 d and 0.58, respectively. The dotted line marks the systemic velocity.

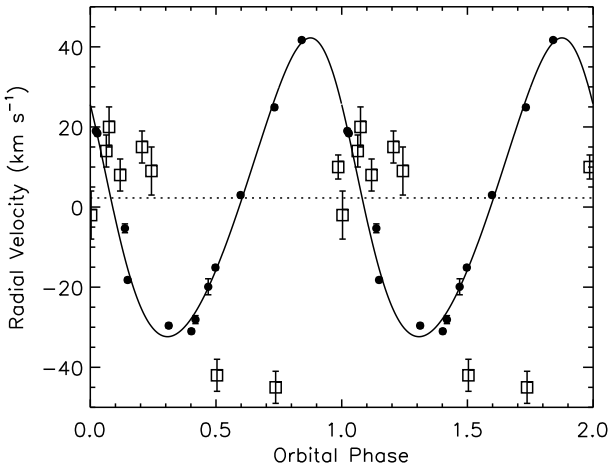

Figure 7. Radial velocity curve and orbital solution for the SB1 HDE 305536 at the best-fitting orbital period of 1.88535 d. Solid circles are measurements from our CHIRON spectra. Open squares are data from Levato et al. (1990), shown for comparison but not used to fit the orbital solution. The dotted line marks the systemic velocity.

multi-wavelength photometry is needed to confirm the characteristics of the secondary star.

3.4 HDE 305536

The O9.5 V star (Sota et al. 2014) HDE 305536 is located close to the optical center of the open cluster Cr 228 (e.g., Wu et al. 2009), a few pc from the WNH star WR 24. Like HD 93576, it is associated with an extended arc of 8 μm emission indicative of a stellar wind bow shock, which in this case points in the general direction of Tr 16 (Sexton et al. 2015). HDE 305536 was observed multiple times by Levato et al. (1990), who detected significant RV variations and fit a rough orbit with a period of 2.018 d.

We obtained 12 CHIRON spectra of this system over 2014–2016. The parameters of the best-fitting orbital solution to our data, which has a period of 1.88535 ± 0.00002 d, are given in Table 4 and the corresponding phase-folded RV curve is shown in Figure 7. `rvfit` was unable to converge on a solution when the RVs from Levato et al. (1990) were included; we overplot those data, folded at our best-fitting CHIRON-based period, for comparison only. Relative to our CHIRON measurements, the Levato et al. (1990) data appear offset by 10–30 km s^{-1} in RV and/or 0.2–0.3 in phase. As discussed in Section 2.4, many Levato et al. (1990) sources show unexplained RV offsets relative to later observations. In this case, the apparent phase shift may also suggest the possibility of orbital precession.

The orbit of HDE 305536 is slightly eccentric with $e = 0.129 \pm 0.008$. The mass function of the system is $f(M_1, M_2) \approx 0.01$ M$_\odot$. Assuming the mass of the O9.5 V primary star is $\sim$ 16 M$_\odot$ (Martins et al. 2005), the minimum mass of the secondary star is $\sim$ 1.4 M$_\odot$, equivalent to a mid F-type dwarf (Drilling & Landolt 2000).

3.5 Additional spectroscopic binaries

In addition to HD 93403 and the four spectroscopic binaries described above, six other stars showed significant ($P(\chi^2, \nu) < 0.01$) RV variations with amplitudes > 20 km s^{-1}. These variations are larger than typical photospheric variability (e.g., Martins et al. 2015), making these stars probable but unconfirmed spectroscopic binaries. We briefly discuss each of these sources below.

ALS 15204: There are no literature RV data for this O7.5 V star (Sota et al. 2014) in Tr 14. We observed it three times with CHIRON in 2014. In spectra taken 16 days apart, its RV changed by more than 100 km s^{-1}. Owing to this star's relative faintness (V = 10.9 mag; Hur et al. 2012), we did not pursue follow-up observations in 2015.

ALS 15206: We observed ALS 15206, an O9.2 V star (Sota et al. 2014) in Tr 14, a total of three times with CHIRON in Dec 2014. Our observations show variability that is significant but low-amplitude (ΔRV$\sim$ 10 km s^{-1}). However, its single-epoch RV from Huang & Gies (2006) is $\sim$ 30 km s^{-1} blueshifted relative to our CHIRON numbers, suggesting a higher degree of variability. ALS 15206 is associated with an extended arc of 8 μm emission, likely a stellar wind bow shock, that points northwest toward the center of Tr 14 (Sexton et al. 2015). It has a local proper motion of $\lesssim$ 30 km s^{-1}, directed to the northeast (Kiminki et al. 2017). As with ALS 15204, we did not pursue follow-up CHIRON observations because this star is relatively faint at visual magnitudes (V = 10.7 mag; Hur et al. 2012)

ALS 15207: This O9 V star (Sota et al. 2014) in Tr 14 was flagged by Levato et al. (1991b) as an SB2; however, García et al. (1998) observed no line doubling nor any significant RV variations. We obtained a total of seven CHIRON spectra of ALS 15207 in 2014–2015; like García et al. (1998), we found that its He I and He II absorption lines were well fit with single Gaussian profiles. We measured RVs ranging from −21.5 km s^{-1} to +15.0 km s^{-1} but were unable to constrain the period of the variability.

CPD-59 2554: Although this O9.5 IV star (Sota et al. 2014) in Cr 228 was observed by Levato et al. (1990) to be a constant-RV source, our nine CHIRON spectra from 2014–2015 show significant variability, with RVs ranging from −22.7 km s^{-1} to +63.4 km s^{-1}. We were unable to constrain the period of the variability.

HD 93028: This O9 IV star (Sota et al. 2014) is located about 6 pc southwest of the center of Cr 228. Levato et al. (1990) identified it as a spectroscopic binary and fit a rough orbit with a pe-

riod of 51.554 d. We obtained four CHIRON spectra of this source in 2014, which showed significant RV variations at an amplitude just above our 20 km s^{-1} cutoff; a larger amplitude is seen when data from Feast et al. (1957) and Conti et al. (1977) are included. Sota et al. (2014) report that HD 93028 is in a long-period ($\sim$ 200 d) spectroscopic binary, but do not provide an orbital solution.

HDE 305525: At about 7 pc southwest of Tr 16, this O5.5 V star (Sota et al. 2014) is part of the distributed population in the South Pillars. Levato et al. (1990) detected significant RV variability in its spectra but were unable to find an orbital solution. Our eight CHIRON spectra from 2014–2015 confirm RV variations with an amplitude of more than 130 km s^{-1}. Like Levato et al. (1990), we were unable to constrain the period of the variability.

4 RESULTS AND DISCUSSION

4.1 Distribution of stellar radial velocities

Combining new spectroscopy with literature data, we have compiled heliocentric RVs for 59 O-type systems in the Carina Nebula, as well as for the LBV η Car and the three WNH stars in the region. We present a histogram of these RVs in Figure 8. The stars are divided into three groups, characterizing the likelihood that the observed RVs represent their true systemic motions. The first group, shown in light gray in Figure 8, are sources with relatively reliable RVs. These are spectroscopic binaries with well-constrained orbital solutions, for which we plot the computed systemic velocity, as well as stars with no known RV variability or insignificant or low-amplitude RV variability, for which we plot the weighted mean of the observed RVs. In total, this group, which we will henceforth refer to as the "well-constrained sources," consists of η Car and 40 O-type stars. The weighted mean RV of the well-constrained sources is 0.6 km s^{-1}, with a standard deviation of 9.1 km s^{-1}.

The second group of sources, shown in dark gray in Figure 8, are those that have been identified as spectroscopic binaries but lack orbital solutions. These include stars that were identified as SB1s or SB2s in the multiplicity survey of Chini et al. (2012), stars with binarity flagged elsewhere in the literature, and stars whose CHIRON and/or literature RVs display significant variability with amplitudes > 20 km s^{-1}. We refer to this group of 19 O-type systems as the "unsolved binaries." For each system, we plot the weighted mean of its measured RVs, but caution that this number may not be representative of its true systemic velocity, especially for systems with few published RVs. For instance, the most notable outlier in Figure 8 is HD 93130, for which there is only a single reliable published RV (59.9 km s^{-1}; Conti et al. 1977). However, Chini et al. (2012) classify this source as an SB2, suggesting that its outlying single-epoch RV is the result of its binarity rather than its relationship with the Carina Nebula. The overall weighted mean RV of the well-constrained sources and the unsolved binaries together remains 0.6 km s^{-1}, while the standard deviation of the distribution increases to 13.5 km s^{-1}.

The third group of sources, shown in black in Figure 8, are the WNH stars. As discussed in Section 2.4, the N IV λ4058 RVs adopted for these sources are affected by their strong stellar winds. All three fall on the negative end of the Carina Nebula's RV distribution, offset by roughly -30 km s^{-1} from the mean velocity of the O-type systems. We cannot rule out the possibility that the WNH stars are a distinct kinematic group or that one or more of them is moving at outlying speeds after having been ejected from the region's clusters. However, given that the three stars show a similar RV offset, wind effects are most likely the primary cause.

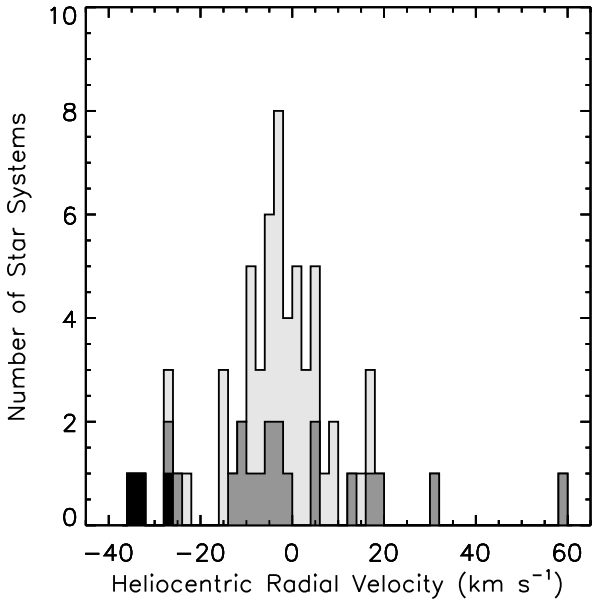

Figure 8. Histogram of the heliocentric radial velocities of the O-type and evolved massive stars in the Carina Nebula. Well-constrained sources (solved spectroscopic binaries and stars with little to no RV variation) are shown in light gray. Unsolved binaries are shown in dark gray. The three WNH stars, whose reported RVs are affected by strong stellar winds, are indicated in black.

The overall RV distribution in Figure 8 is unimodal, consistent with the various clusters and subclusters of the Carina Nebula being part of a single complex at a common distance. We do not see any probable runaway stars. Aside from WR 24 and WR 25, only HD 93130 has an RV that deviates from the region's mean by $\geq$ 30 km s^{-1}, and as described above, HD 93130 is a poorly-studied spectroscopic binary and its given RV is unlikely to be its true systemic velocity. However, with RV data, we cannot rule out the presence of runaways with high tangential velocities. Our region of study extends $\sim$ 20 pc in all directions from Tr 16, meaning a star with a tangential velocity of 30 km s^{-1} would have exited our field in $\sim$ 600,000 yr. An O-type star ejected by the recent supernova explosion of its companion (see, e.g., Blaauw 1961) might still appear to be within the coordinates of the Carina Nebula, but we see no evidence for this in the RV data.

The standard deviation of the RVs of the well-constrained sources, 9.1 km s^{-1}, is an upper limit on the true one-dimensional velocity dispersion of the Carina Nebula, as this group of sources may still contain long-period spectroscopic binaries or other undetected RV variables. Typical OB associations like Scorpius-Centaurus and Perseus OB2 have one-dimensional velocity dispersions of 1–3 km s^{-1} (de Bruijne 1999; Steenbrugge et al. 2003), but these associations are substantially smaller in mass and extent—and slightly older—than the Carina Nebula complex (see Bally 2008; Preibisch & Mamajek 2008). More directly comparable to the Carina Nebula is the Cygnus OB2 association, which contains > 50 O-type stars distributed across tens of parsecs (Massey & Thompson 1991; Wright et al. 2015). In both tangential and radial velocities, the one-dimensional velocity dispersion of Cyg OB2 is $\sim$ 10 km s^{-1} (Kiminki et al. 2007, 2008; Wright et al. 2016), similar to what we have measured for the O-type stars in the Carina Nebula. This is about a factor of two higher than the velocity dispersions seen in the massive, compact starburst clusters R136

(Hénault-Brunet et al. 2012), NGC 3603 (Rochau et al. 2010), and the Arches Cluster (Clarkson et al. 2012).

4.2 Variations between clusters

In Figure 9, we separate out and compare the RVs of the O-type and evolved massive stars in Tr 14 and Tr 16. We define membership in each cluster as being within a projected 5′ of the cluster center. This is the observed radius of Tr 14's pre-main-sequence population (Ascenso et al. 2007) and a natural break in its O-star distribution. Tr 14 contains six O-type stars with well-constrained RVs and an additional nine unsolved binaries. Tr 16 is larger and less well-defined than Tr 14, and is elongated rather than spherical (e.g., Feigelson et al. 2011), and so is poorly defined by a single radius. With a 5′ cutoff, Tr 16 contains 11 sources with well-constrained RVs (including η Car), and three unsolved binaries. As we describe below, increasing the radius of Tr 16 slightly increases its velocity dispersion but has little effect on the weighted mean of its RV distribution.

The cumulative histograms in Figure 9 suggest that the O-type stars in Tr 14 might have slightly more positive RVs, on average, than those in Tr 16. The weighted mean of the well-constrained sources in Tr 14 is 2.3 ± 7.4 km s^{-1}, in agreement with the 2.8 ± 4.9 km s^{-1} measured by Penny et al. (1993) and the 6.0 ± 1.4 km s^{-1} found by García et al. (1998). In comparison, the weighted mean of the well-constrained sources within a 5′ radius of Tr 16 is −3.5 ± 8.6 km s^{-1}. Increasing the radius of Tr 16 to 10′ changes this to −3.3 ± 10.4 km s^{-1}. To evaluate the significance of the apparent RV difference between clusters, we ran a two-sided Kolmogorov-Smirnov (K-S) test, which evaluates the probability that the two clusters were drawn from the same RV distribution. We estimated the uncertainty on the K-S probability by drawing 10^4 combinations of each cluster's RVs, randomly permuting each star's RV within a Gaussian distribution with a standard deviation corresponding to that star's observed RV uncertainty. For the well-constrained sources (the top panel of Figure 9), the probability that the two clusters come from the same RV distribution is 4^{+19}_{-3}%, meaning the difference in RVs is marginally significant. Including unsolved binaries (as in the bottom panel of Figure 9) brings the probability of a shared RV distribution to 16^{+45}_{-13}%, indicating that the difference is not significant. Further study of the kinematics of Tr 14 and Tr 16 are needed to determine if any overall RV difference persists in their lower-mass stellar populations. Damiani et al. (2017) found a mean RV of −5 km s^{-1} for the FGK-type populations of Tr 14 and Tr 16 combined, with no apparent bimodality in their RV distribution, but they did not attempt to separate their stars by cluster.

In Figure 10, we search for any additional cluster-scale or spatial dependencies by mapping our RVs as a function of position. The circle representing each star is scaled by the magnitude of its mean/systemic RV and color-coded as redshifted (positive RV) or blueshifted (negative RV). The left-hand plot includes only those sources with well-constrained RVs, while the right-hand plot shows both the well-constrained sources and the unsolved binaries. For clarity, we mark only the positions and not the RVs of the three WNH stars.

The apparent velocity difference between Tr 14 and Tr 16 is visible in Figure 10, in that the former has more red (positive-RV) sources than the latter. Another notable structure is the grouping of O-type stars extending from the nominal center of Cr 228 up toward Tr 16. These sources have low-magnitude RVs and appear as a sequence of relatively small circles. Their weighted mean RV (0.3 km s^{-1}) is similar to that of the region as a whole, but their velocity dispersion (4.0 km s^{-1}) is comparatively small. This relatively low velocity dispersion suggests that this string of massive stars formed in place; we would expect a population that had migrated out from Tr 16 to have a higher velocity dispersion than the cluster rather than vice versa.

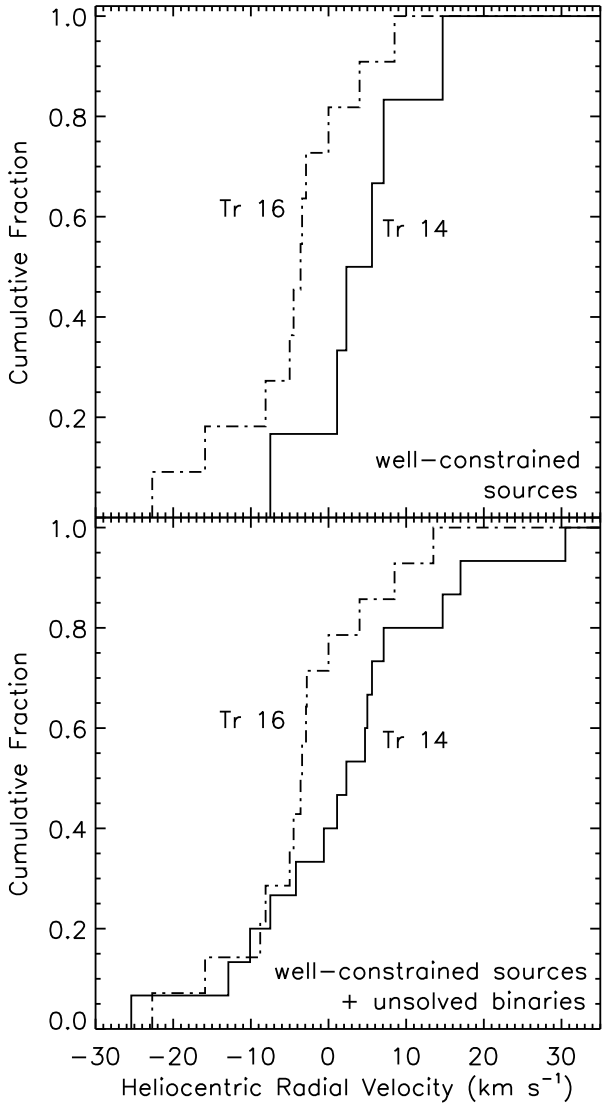

Figure 9. Cumulative histograms of the heliocentric radial velocities of O-type stars in Tr 14 (solid line) and O-type stars and η Car in Tr 16 (dot-dash line). Both clusters are defined with a radius of 5′. Top: stellar systems with well-constrained RVs (either solved spectroscopic binaries or sources with little to no RV variation). Bottom: as above, but including the mean RVs of unsolved spectroscopic binaries.

4.3 Comparison to molecular gas

The molecular cloud complex associated with the Carina Nebula is composed of three main parts (de Graauw et al. 1981; Brooks et al. 1998; Yonekura et al. 2005; Rebolledo et al. 2016). The Northern Cloud partially surrounds Tr 14 and extends to the northwest (de Graauw et al. 1981; Brooks et al. 2003), where it connects to additional molecular material around the Gum 31 H II region (e.g., Rebolledo et al. 2016). The Southern Cloud coincides

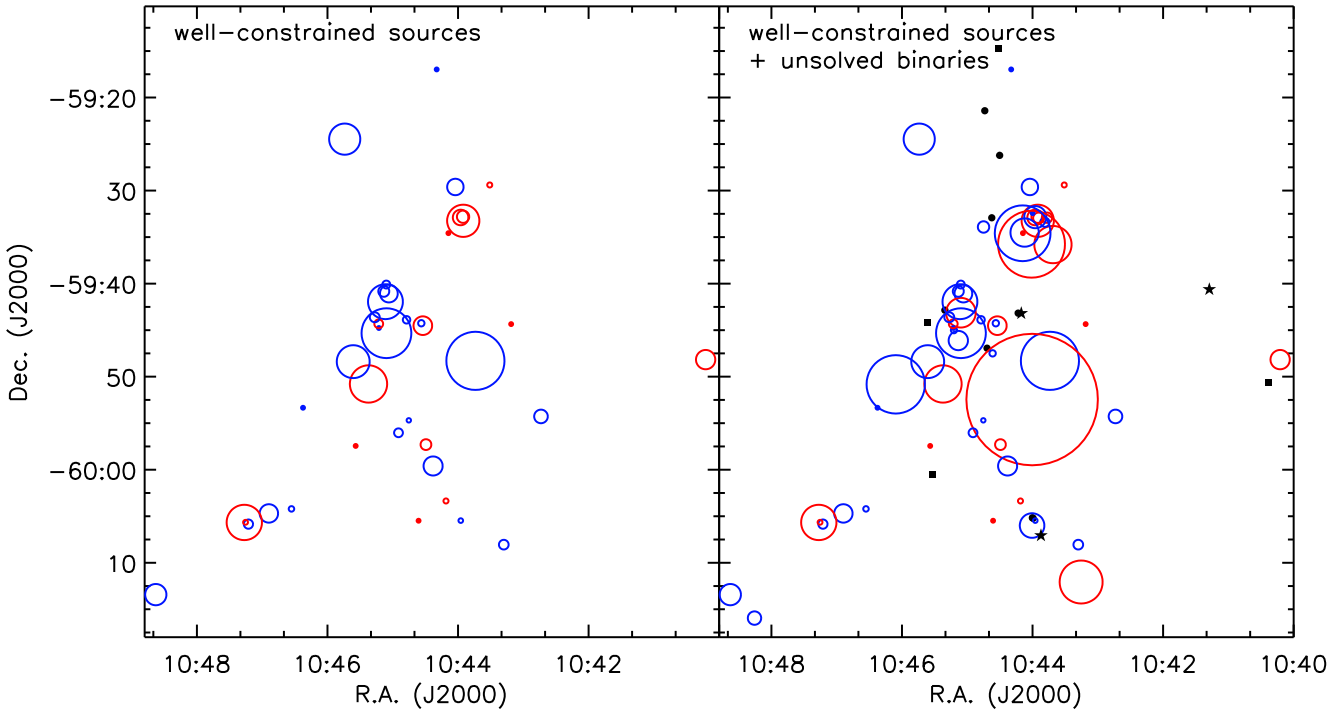

Figure 10. Maps of the heliocentric radial velocities of O-type and evolved massive stars in the Carina Nebula. Left: stars (including η Car) with well-constrained RVs as defined in the text. Blue circles indicate negative RVs and red circles indicate positive RVs; circle size scales with the magnitude of the velocity. Right: as left, but including known spectroscopic binaries that lack orbital solutions. The filled black circles and squares show the positions of O-type stars from v3.1 of the GOSC and from Alexander et al. (2016), respectively, that lack RV data. The positions of the three WNH stars are shown by black filled stars.

with the optically dark lane between Tr 16 and the South Pillars (de Graauw et al. 1981). The South Pillars are themselves composed of molecular gas, shaped by feedback from Carina's OB stars (Rathborne et al. 2004; Yonekura et al. 2005; Rebolledo et al. 2016). Within Tr 16 there are only scattered molecular globules, thought to be the remnants of the gas from which that cluster formed (Cox & Bronfman 1995; Brooks et al. 2000).

Rebolledo et al. (2016) observed the Carina Nebula in ^{12}CO (1–0) emission as part of the Mopra Southern Galactic Plane CO Survey (Burton et al. 2013). We use their data to compare the kinematics of Carina's molecular gas to the RVs of its O-type and evolved massive stars. For Figures 11 and 12, we collapse their three-dimensional data cubes along Galactic latitude and Galactic longitude, respectively, to present two-dimensional position–velocity diagrams of the dense gas in Carina. We convert the gas velocities from the Local Standard of Rest to a heliocentric frame. At the coordinates of the Carina Nebula, $RV_{\rm helio} \approx RV_{\rm LSR} + 11.6$ km s^{-1}. All RVs in the following discussion are heliocentric unless otherwise noted.

Figure 11 plots the RVs of the Carina Nebula's O-type stars, evolved massive stars, and ^{12}CO (1–0) emission as a function of Galactic longitude l. The ^{12}CO fluxes from Rebolledo et al. (2016) are summed across Galactic latitudes $-1.4 \leq b \leq 0.1°$. As in Figure 8, the stars are divided into three groups: stars (including η Car) with well-constrained systemic velocities, unsolved binaries, and WNH stars. We also indicate the approximate heliocentric velocities of the redshifted and blueshifted components of ionized gas emission lines observed by Damiani et al. (2016) for shells centered on the locations of η Car, WR 25, and Tr 14. In Figure 12, we present the same data, but plotted as a function of Galactic latitude b. The ^{12}CO fluxes are summed across Galactic longitudes $287.0 \leq l \leq 288.4°$.

The three components of Carina's molecular cloud complex separate cleanly when plotted against Galactic latitude in Figure 11: the Northern Cloud at $l \approx 287.0$–$287.5°$ with heliocentric RV $\approx (-10)$–0 km s^{-1}; the Southern Cloud at $l \approx 287.6$–$287.8°$ with heliocentric RV $\approx (-15)$–(-10) km s^{-1}; and the South Pillars at $l \approx 287.9$–$288.2°$ with heliocentric RV $\approx (-10)$–(-5) km s^{-1} and a smaller part at $\sim$ 0 km s^{-1}. The separation is less notable in Figure 12, as the sourthern part of the Northern Cloud overlaps with the Southern Cloud in Galactic longitude, but the RV offset in the Southern Cloud is still apparent. The molecular gas at $l \approx 287.7$–$287.8°$, $b \approx -0.4$, with heliocentric RV $\sim +20$ km s^{-1}, is thought to be associated with the far side of the Carina arm, at a greater distance than the Carina Nebula (Damiani et al. 2016).

Figures 11 and 12 further emphasize that the RVs of the O-type stars in the Carina Nebula are not spatially dependent, as there is no trend in O-star RVs with Galactic longitude or latitude. Rebolledo et al. (2016) applied the four-arm Milky Way model of Vallée (2014) to the rotation curve of McClure-Griffiths & Dickey (2007) and calculated the expected RV for objects at various distances along the tangent of the Carina spiral arm. For sources on the near side of the arm, at $\sim$ 2 kpc, the expected Local Standard of Rest RV is approximately -10 km s^{-1}, which corresponds to a heliocentric RV of $\approx +2$ km s^{-1}, very close to the observed mean RV of the O-type stars. Objects at greater distances from the Sun would be expected to have more positive RVs (see Rebolledo et al.

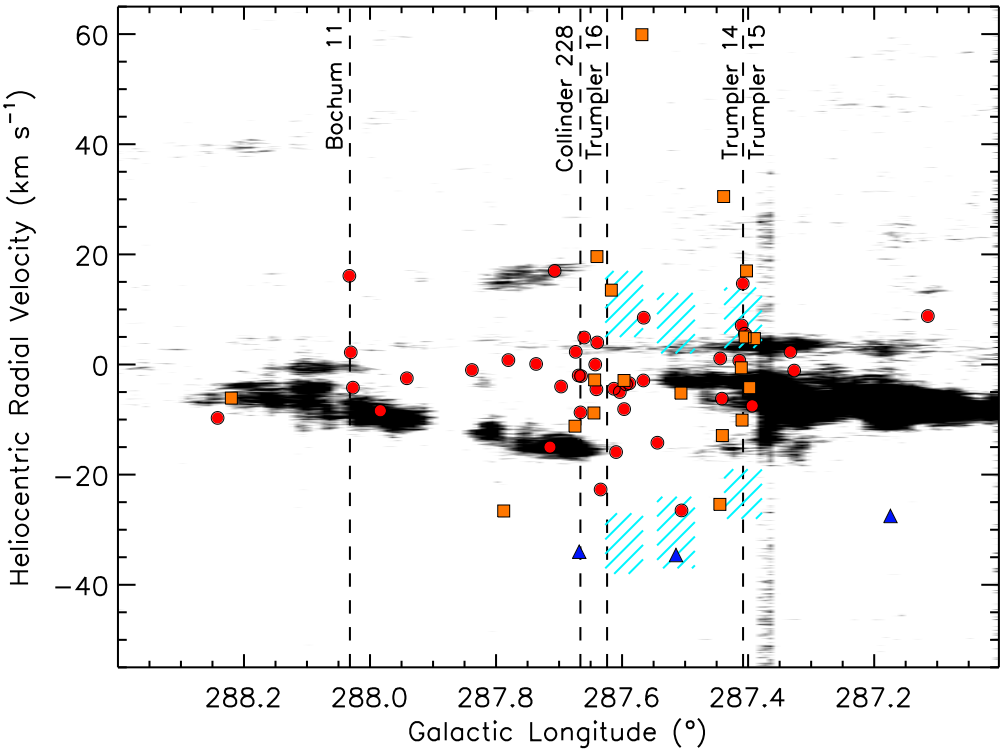

Figure 11. Position-velocity diagram of ^{12}CO (1–0) emission (gray-scale) from Rebolledo et al. (2016, converted to a heliocentric frame) compared to O-type and massive evolved stars. Red circles are systems (including η Car) with well-constrained radial velocities, orange squares are known or suspected spectroscopic binaries that lack orbital solutions, and blue triangles are WNH stars. The hatched cyan regions show the RVs of the approaching and receding components of emission from ionized gas (Damiani et al. 2016) centered on the positions of η Car, WR 25, and Tr 14.

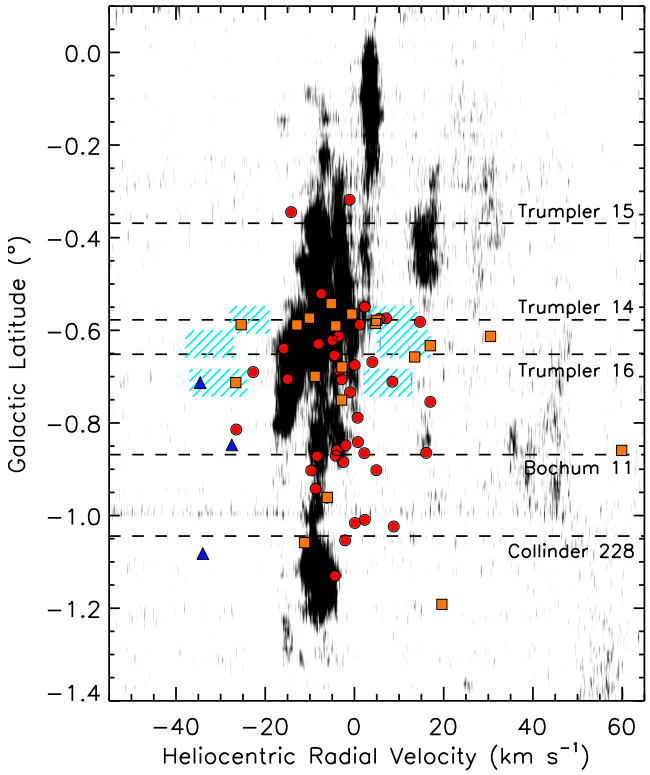

Figure 12. Similar to Figure 11, but showing the heliocentric radial velocities of ^{12}CO, ionized gas, and stars as a function of Galactic latitude.

2016). Our RV results thus favor the OB clusters and groups in the Carina Nebula being at a common distance of approximately 2 kpc.

4.3.1 *Tr 14, Tr 15, and the Northern Cloud*

There is a general consensus that the relatively compact Tr 14 is the youngest of the Carina Nebula's Trumpler clusters, at just 1–2 Myr old (Walborn 1973, 1982a,b, 1995; Morrell et al. 1988; Vazquez et al. 1996; Smith & Brooks 2008; Rochau et al. 2011). The case for its youth is strengthened by its close spatial association with the Northern Cloud, which wraps around the west side of the cluster (de Graauw et al. 1981; Brooks et al. 2003; Tapia et al. 2003). Bright radio emission arises from multiple ionization fronts where radiation from Tr 14 impacts dense clumps in the Northern Cloud (Whiteoak 1994; Brooks et al. 2001). It is clear from Figures 11 and 12 that the O-type stars in Tr 14 are also kinematically associated with the Northern Cloud, further strengthening the picture of Tr 14 as a young cluster that has not yet dispersed its natal molecular gas.

While Tr 15 has sometimes been considered an unrelated foreground or background cluster (Thé & Vleeming 1971; Walborn 1973), its extended X-ray stellar population indicates a connection to Tr 14 (Feigelson et al. 2011; Wang et al. 2011). We have RV data for only two O-type stars around Tr 15, HD 93403 and HD 93190, which appear at $b \sim -0.35°$ in Figure 12. Their RVs are consistent with those of the rest of the O-type stars in the Carina Nebula, and span the RV range of the Northern Cloud. Both are 4–5 pc outside the core of Tr 15, and neither is associated with any group or subcluster (see Feigelson et al. 2011). Tr 15 is likely several Myr older than Carina's other Trumpler clusters (Carraro 2002; Tapia et al.

2003; Wang et al. 2011), and it seems likely that these two stars drifted out from Tr 15 over the course of their lifetimes.

Off the southern edge of the Northern Cloud, on the far west side of the Carina Nebula (see Figure 1), there are several O-type and evolved massive stars, notably WR 22 and HD 92607. There is a young (< 1 Myr) pre-main-sequence population in this region, although it does not show any clustering around the massive stars (Kumar et al. 2014). WR 22 is a particularly puzzling system: it is a very massive binary (~55-$M_\odot$ primary; Schweickhardt et al. 1999) approximately 21′ (15 pc) from Tr 14, without any subcluster or group of its own. Its N IV λ4058 RV is somewhat less negative than the RVs of WR 24 and WR 25, but it is unclear whether this represents a true difference in their systemic motions or whether it is the result of uncharacterized differences in their stellar winds.

The SB2 HD 92607 (see Section 3.1), evident on the far right side of Figure 11, is less extreme in mass but still somewhat puzzling in origin. Its systemic RV (8.8 km s^{-1}) is relatively positive for an O-type system in the Carina Nebula, although still within one standard deviation of the mean. And despite its proximity to the Northern Cloud, it lacks a kinematic association with the molecular gas—perhaps a hint that it did not form in its currently observed location. HD 92607 is associated with a candidate bow shock in the form of a resolved 24 μm arc pointing to the southeast (Sexton et al. 2015), which might suggest an origin outside the Carina Nebula. However, in the active environment of this giant H II region, bow shocks are not clear indicators of stellar motion (Kiminki et al. 2017). Its spectroscopic parallax (using data from Martins et al. 2005; Gagné et al. 2011; Povich et al. 2011b) and the inferred distance from its *Gaia* DR1 geometric parallax (Astraatmadja & Bailer-Jones 2016) are both consistent with HD 92607 being part of the Carina Nebula at a distance of around 2 kpc.

4.3.2 *Tr 16 and the Southern Cloud*

Unlike the Northern Cloud, which has a close kinematic association with the Tr 14 cluster, the Southern Cloud is offset by 10–15 km s^{-1} in RV from its neighbor Tr 16. The Southern Cloud has the most negative RVs of the molecular gas in Carina, being 5–10 km s^{-1} blueshifted relative to both the Northern Cloud and the molecular gas in the South Pillars. It coincides with a prominent, optically dark dust lane, indicating that it lies in front of the southeastern edge of Tr 16 (Dickel 1974; de Graauw et al. 1981; Brooks et al. 1998). Inside Tr 16 itself, there are only small clumps of molecular gas (not visible in the Rebolledo et al. 2016 data), and these have RVs more consistent with those of the O-type stars in the cluster (Cox & Bronfman 1995; Brooks et al. 2000).

One of the key arguments in favor of Tr 16 being 1–2 Myr older than Tr 14 (e.g., de Graauw et al. 1981; Walborn 1995) is that the latter (in addition to being more compact) is still partially enclosed by its natal molecular cloud, while the former appears to have disrupted the gas from which it formed. The distribution of gas RVs in Figure 11 suggests that the Northern Cloud, Southern Cloud, and Southern Pillars were originally part of a single continuous molecular cloud, with the massive stars in Tr 16 having since blown out the central part of that cloud. The Northern Cloud, currently being eroded by Tr 14, has not been accelerated along our line-of-sight, while the molecular gas in the South Pillars has undergone some acceleration at its closest approach to Tr 16.

The acceleration of the Southern Cloud by the O-type stars in Tr 16 is readily explained by the rocket effect (Oort & Spitzer 1955; Bally & Scoville 1980; Bertoldi & McKee 1990). As the neutral gas facing Tr 16 is ionized by the strong ultraviolet radition of the cluster (Smith 2006), it flows away from the surface of the molecular cloud at roughly its sound speed. The recoil force on the molecular cloud causes it to accelerate away from the ionizing source at a rate proportional to the rate at which it loses mass through ionization. In the simplest scenario, assuming the cloud is initially at rest relative to the ionizing source, the cloud mass and velocity are connected through (Spitzer 1978):

$$M_c = M_0 e^{-v_c/V_{\rm ion}}, \quad (1)$$

where M_0 and M_c are the initial and current masses of the molecular cloud, respectively, v_c is the current velocity of the cloud, and $V_{\rm ion}$ is the velocity with which the newly ionized material flows away from the cloud. For the molecular cloud to have been accelerated to ~10 km s^{-1}, roughly the speed of sound in ionized gas, the cloud's mass must have decreased by ~60%. The current mass of the Southern Cloud is ~ 5×10^4 $M_\odot$ (Rebolledo et al. 2016). Accounting only for mass loss through ionization, its initial mass would have been on the order of 1.3×10^5 $M_\odot$, comparable to the current mass of the Northern Cloud (Yonekura et al. 2005; Rebolledo et al. 2016).

Noteworthy among the O-type stars in Tr 16 is V662 Car at $l = 287.7°$, $b = -0.7°$, an eclipsing spectroscopic binary with a systemic velocity of -15 ± 2 km s^{-1} (Niemela et al. 2006). V662 Car is the only O-type star to coincide with the Southern Cloud in three-dimensional position–velocity space, and its relatively high visual extinction (Smith 1987; Povich et al. 2011a) suggests that it is behind or within the molecular gas. The primary star's spectrum has unusually strong He II λ4686 (Niemela et al. 2006), leading it to be assigned to the luminosity class Vz (Sota et al. 2014), which is associated with very young O-type stars close to the zero-age main sequence (Walborn 2009; Sabín-Sanjulián et al. 2014; Walborn et al. 2014; Arias et al. 2016). Roughly a dozen of the O-type stars in the Carina Nebula are of class Vz (Sota et al. 2014), with the highest fraction relative to non-z O dwarfs found in Tr 14 (Arias et al. 2016). In addition, Niemela et al. (2006) found that both components of V662 Car have smaller radii and luminosities than expected for their spectral types, another indicator of youth. The combination of V662 Car's young age, its deviation from the mean RV of the O-type stars in Tr 16, and its kinematic association with the Southern Cloud suggest that it was formed separately from and more recently than the body of Tr 16. We propose that its formation may have been triggered by the feedback-induced acceleration of the Southern Cloud.

4.3.3 *Cr 228, Bo 11, and the molecular gas in the South Pillars*

The relationship between the O-type stars in Bo 11 and Cr 228 and the molecular gas in the South Pillars is difficult to interpret, because the gas detected in ^{12}CO is spatially separate from the O-type stars. Most of the ^{12}CO (1–0) emission in the South Pillars comes from the so-called Giant Pillar (Smith et al. 2000; Yonekura et al. 2005; Smith et al. 2010b), a dusty structure that points toward Tr 16 from the southernmost part of the region, lying roughly halfway between Bo 11 and the nominal center of Cr 228. The Giant Pillar is the site of current star formation (Smith et al. 2010b; Gaczkowski et al. 2013), but is ≥ 4 pc from any O-type stars. Its gas has heliocentric RVs of (−10)–(−5) km s^{-1}, similar to the Northern Cloud. Another dusty structure, whose ionization fronts also face Tr 16, is spatially coincident with Bo 11. Some ^{12}CO (1–0) emission, too faint to appear in Figures 11 and 12, is

detected in this region (Rebolledo et al. 2016), but it has a heliocentric RV of $\gtrsim 30$ km s^{-1} and likely belongs to the far side of the Carina spiral arm.

Most of the O-type stars in Bo 11 have RVs similar to the rest of the O-type stars in the Carina Nebula and comparable to the gas in the South Pillars. The exception is HDE 305612, which, with a measured mean RV of 16.1 km s^{-1}, appears to be a notable outlier. However, HDE 305612 shows significant RV variation over three epochs of CHIRON data—but was not flagged as an unsolved binary because the amplitude of that variation is < 20 km s^{-1}.

The O-star population of Cr 228 also has similar RVs to the rest of the region; in Figure 11, it is indistinguishable from the O-star population of Tr 16. None of the many smaller dust pillars around Cr 228 (Smith et al. 2010b) are detected in ^{12}CO (1–0) emission (Rebolledo et al. 2016), ruling out a direct comparison between the RVs of stars and gas in this part of the Carina Nebula. As discussed in Section 4.2, the O-type stars in and around Cr 228 have a lower velocity dispersion than the region as a whole, suggesting that they were not scattered out of Tr 16.

In the far southeast corner of the Carina Nebula, approximately 12.5′ (∼8 pc) from Bo 11, are HD 93843 and HDE 305619. These two stars are clearly visible on the left side of Figure 11 as the two O-type systems with the highest Galactic longitudes. They are typically treated as members of the Carina Nebula complex (e.g., Gagné et al. 2011), although there are no known gas structures or lower-mass stellar populations connecting them to the rest of the South Pillars (e.g., Smith et al. 2010b). The spectroscopic parallax of HDE 305619 (using data from Kharchenko 2001; Martins et al. 2005; Kharchenko & Roeser 2009; Gagné et al. 2011; Sota et al. 2014) suggests that it might be in the background at a distance of > 3 kpc, but inferred distances based on *Gaia* DR1 (Astraatmadja & Bailer-Jones 2016) place both it and HD 93483 at ~ 2.4 kpc. Their observed RVs are also consistent with being part of the Carina Nebula complex, although HDE 305619 shows significant low-amplitude variability in our CHIRON data and was classified as an SB1 by Chini et al. (2012).

4.4 Comparison to ionized gas

The ionized gas in the Carina Nebula is globally expanding at ±15–20 km s^{-1}, as seen in radio recombination lines (Gardner et al. 1970; Huchtmeier & Day 1975; Azcarate et al. 1981; Brooks et al. 2001) and optical line emission (Deharveng & Maucherat 1975; Walborn & Hesser 1975; Walsh 1984; Smith et al. 2004). This expansion is driven by feedback from Carina's O-type and evolved massive stars (Smith & Brooks 2007). It was most recently mapped by Damiani et al. (2016), who observed more than 650 optical sightlines across Tr 14 and Tr 16. They identified three non-spherical expanding shells, roughly centered on the positions of η Car, WR 25, and Tr 14. We represent these shells in Figures 11 and 12 with hatched regions showing the range of observed approaching and receding RVs for each shell. Damiani et al. (2016) estimate that the overall expansion is centered around an RV of -12.5 km s^{-1}. Their Tr 14 shell is centered around a slightly less negative -8 km s^{-1}. These values agree with prior results: Walborn (1973); Walborn et al. (2002b, 2007) place the kinematic center of the expansion at -14 km s^{-1}, and radio data (Gardner et al. 1970; Huchtmeier & Day 1975; Azcarate et al. 1981) consistently centers the expansion at a heliocentric RV of -9 km s^{-1}.

However, the RV distribution of Carina's O-type and evolved massive stars is not aligned with the expansion of the ionized gas. As described in Section 4.1, the weighted mean RV of the well-constrained O-type stars is 0.6 ± 9.1 km s^{-1}, putting the kinematic center of the ionized gas expansion roughly one standard deviation blueward of the mean O-star RV. Figures 11 and 12 show that the receding/redshifted components of the gas overlap in RV space with the positive-RV tail of the O-star distribution, while the approaching/blueshifted components of the gas have more negative RVs than nearly all of the O-type stars. The N IV λ4058 RVs of the WNH stars, including WR 25, agree with the RVs of the approaching gas, but as previously discussed, this is due to wind effects in the WNH spectra and not due to a physical association.

The most likely explanation for the kinematic asymmetry between the gas and the O-type stars is that the receding/redshifted ionized gas is bounded by dense, neutral material behind the Carina Nebula, while the approaching/blueshifted ionized gas moves freely along our line of sight. In addition, the approaching gas around Tr 16 may be partially composed of a photoevaporative flow off the Southern Cloud, which has already been accelerated toward us by feedback from Tr 16 (see Section 4.3.2). Damiani et al. (2016) noted a number of smaller-scale kinematic asymmetries in the ionized gas shells, confirming that the expansion of the H II region is non-spherical and is affected by density variations in the surrounding medium. We consequently caution against using the kinematic center of the ionized gas to define the systemic RV of the Carina Nebula.

5 CONCLUSIONS

We have conducted a radial velocity survey of the O-type and evolved massive stars in the Carina Nebula. We obtained multi-epoch echelle spectroscopy for 31 O-type stars, and compiled published RVs for an additional 32 systems including three WNH stars and the LBV η Car. With these data, we find the first spectroscopic orbital solutions for the near-twin system HD 92607 and the eclipsing binary HDE 303312 and provide updated orbital solutions for HD 93576 and HDE 305536. Our further results are summarized as follows:

(1) Of the 63 O-type and evolved massive star systems with RV data, 41 have well-constrained systemic velocities. These well-constrained sources have a weighted mean RV of 0.6 km s^{-1}, comparable to prior results for the Tr 14 cluster and to the expected radial motion for sources at a distance of ~ 2 kpc along the Carina spiral arm.

(2) The standard deviation of the RVs of the well-constrained sources is 9.1 km s^{-1} and provides an upper limit to the one-dimensional velocity dispersion of the region. This value is high compared to the velocity dispersions of typical, less massive OB associations and is roughly twice that of massive bound starburst clusters. However, it is similar to the velocity dispersion of the large, unbound Cyg OB2 association, and is not unexpected for a region with the content and substructure of the Carina Nebula.

(3) The overall O-star RV distribution is unimodal, favoring a common distance to the various clusters of the Carina Nebula.

(4) There is a possible but marginally significant difference between the RV distributions of the Tr 16 and Tr 14 clusters, with the latter's O-star RVs ~ 5 km s^{-1} more positive, on average, than the former's. Kinematic study of the intermediate-mass populations in these clusters is needed to confirm the offset.

(5) We do not detect any line-of-sight runaway O-type stars, nor do we see evidence that the distributed O-type population migrated out from Tr 14 and Tr 16. On the contrary, the O-type stars

in Cr 228 and the South Pillars have a low velocity dispersion compared to the region as a whole.

(6) The Tr 14 cluster is kinematically associated with the molecular gas of the Northern Cloud, consistent with its young age.

(7) Feedback from Tr 16 has accelerated the molecular gas of the Southern Cloud toward us, relative to the stellar population, by 10–15 km s^{-1}. V662 Car, an O-type star on the outskirts of Tr 16, may belong to a younger generation of stars triggered by this feedback.

(8) The approaching components of the ionized gas around Tr 14 and Tr 16 show higher velocities, relative to the O-type stars, than the receding components. This kinematic asymmetry indicates that the expansion of the H II region is not spherical and is likely impacted by the distribution of dense neutral gas.

Our observations set the stage for the analysis of future *Gaia* data releases, which will add further kinematic dimensions to our understanding of the Carina Nebula. This region continues to be a laboratory for the study of massive-star formation and the interplay between stellar feedback and the interstellar medium.

ACKNOWLEDGEMENTS

We would like to thank the operators of the CTIO 1.5-m telescope for executing our CHIRON observations, and SMARTS Data/Queue Manager Emily MacPherson for queue scheduling. We also thank Maxwell Moe for his guidance in using `NIGHTFALL` to fit the orbit of HDE 303312, and we thank the anonymous referee for the time spent reviewing this manuscript. This work is based on observations at Cerro Tololo Inter-American Observatory, National Optical Astronomy Observatory (NOAO Prop. IDs: 2014B-0235 and 2015B-0141; PI: M. Kiminki), which is operated by the Association of Universities for Research in Astronomy (AURA) under a cooperative agreement with the National Science Foundation. This paper also makes use of data obtained using the Mopra radio telescope, a part of the Australia Telescope National Facility which is funded by the Commonwealth of Australia for operation as a National Facility managed by CSIRO.

Finally, we note that while editing the final revision of this manuscript, we learned of the passing of Nolan R. Walborn. His contributions toward our understanding of massive O-type stars in general have been tremendous, and particularly so for the massive stars in the Carina Nebula studied in this paper.

REFERENCES

Albacete Colombo J. F., Morrell N. I., Niemela V. S., Corcoran M. F., 2001, MNRAS, 326, 78
Albacete Colombo J. F., Morrell N. I., Rauw G., Corcoran M. F., Niemela V. S., Sana H., 2002, MNRAS, 336, 1099
Alexander M. J., Hanes R. J., Povich M. S., McSwain M. V., 2016, AJ, 152, 190
Allen D. A., 1979, MNRAS, 189, 1P
Allen D. A., Hillier D. J., 1993, Proceedings of the Astronomical Society of Australia, 10, 338
Almeida L. A., et al., 2017, A&A, 598, A84
Arias J. I., et al., 2016, AJ, 152, 31
Ascenso J., Alves J., Vicente S., Lago M. T. V. T., 2007, A&A, 476, 199
Astraatmadja T. L., Bailer-Jones C. A. L., 2016, ApJ, 833, 119
Azcarate I. N., Cersosimo J. C., Colomb F. R., 1981, Rev. Mex. Astron. Astrofis., 6, 269
Bally J., 2008, in Reipurth B., ed., , Handbook of Star Forming Regions, Volume I. ASP, San Francisco, CA, p. 459
Bally J., Scoville N. Z., 1980, ApJ, 239, 121
Barbá R. H., Gamen R., Arias J. I., Morrell N., Maíz Apellániz J., Alfaro E., Walborn N., Sota A., 2010, in Rivinius T., Curé M., eds, Revista Mexicana de Astronomia y Astrofisica Conference Series Vol. 38, The Interferometric View on Hot Stars. pp 30–32
Bertoldi F., McKee C. F., 1990, ApJ, 354, 529
Blaauw A., 1961, Bull. Astron. Inst. Netherlands, 15, 265
Bohannan B., Garmany C. D., 1978, ApJ, 223, 908
Brooks K. J., Whiteoak J. B., Storey J. W. V., 1998, Publ. Astron. Soc. Australia, 15, 202
Brooks K. J., Burton M. G., Rathborne J. M., Ashley M. C. B., Storey J. W. V., 2000, MNRAS, 319, 95
Brooks K. J., Storey J. W. V., Whiteoak J. B., 2001, MNRAS, 327, 46
Brooks K. J., Cox P., Schneider N., Storey J. W. V., Poglitsch A., Geis N., Bronfman L., 2003, A&A, 412, 751
Burton M. G., et al., 2013, Publ. Astron. Soc. Australia, 30, e044
Carraro G., 2002, MNRAS, 331, 785
Carraro G., Patat F., 2001, A&A, 379, 136
Carraro G., Romaniello M., Ventura P., Patat F., 2004, A&A, 418, 525
Chini R., Hoffmeister V. H., Nasseri A., Stahl O., Zinnecker H., 2012, MNRAS, 424, 1925
Clark P. C., Bonnell I. A., Zinnecker H., Bate M. R., 2005, MNRAS, 359, 809
Clarkson W. I., Ghez A. M., Morris M. R., Lu J. R., Stolte A., McCrady N., Do T., Yelda S., 2012, ApJ, 751, 132
Coelho P. R. T., 2014, MNRAS, 440, 1027
Collado A., Gamen R., Barbá R. H., 2013, A&A, 552, A22
Collado A., Gamen R., Barbá R. H., Morrell N., 2015, A&A, 581, A49
Conti P. S., Leep E. M., Lorre J. J., 1977, ApJ, 214, 759
Conti P. S., Niemela V. S., Walborn N. R., 1979, ApJ, 228, 206
Cox P., Bronfman L., 1995, A&A, 299, 583
Crowther P. A., 2007, ARA&A, 45, 177
Cudworth K. M., Martin S. C., Degioia-Eastwood K., 1993, AJ, 105, 1822
Damiani F., et al., 2016, A&A, 591, A74
Damiani F., et al., 2017, A&A, 603, A81
Davidson K., Humphreys R. M., 1997, ARA&A, 35, 1
Davidson K., Smith N., Gull T. R., Ishibashi K., Hillier D. J., 2001, AJ, 121, 1569
Deharveng L., Maucherat M., 1975, A&A, 41, 27
Dickel H. R., 1974, A&A, 31, 11
Doran E. I., et al., 2013, A&A, 558, A134
Drilling J. S., Landolt A. U., 2000, in Cox A. N., ed., , Allen's Astrophysical Quantities. Springer, pp 381–396
Efremov Y. N., Elmegreen B. G., 1998, MNRAS, 299, 643
Feast M. W., Thackeray A. D., Wesselink A. J., 1957, Mem. RAS, 68, 1
Feigelson E. D., et al., 2011, ApJS, 194, 9
Feinstein A., Marraco H. G., Muzzio J. C., 1973, A&AS, 12, 331
Feinstein A., Marraco H. G., Forte J. C., 1976, A&AS, 24, 389
Forte J. C., 1978, AJ, 83, 1199
Fullerton A. W., Gies D. R., Bolton C. T., 1996, ApJS, 103, 475
Fullerton A. W., Massa D. L., Prinja R. K., Owocki S. P., Cranmer S. R., 1997, A&A, 327, 699
Gaczkowski B., Preibisch T., Ratzka T., Roccatagliata V., Ohlendorf H., Zinnecker H., 2013, A&A, 549, A67
Gagné M., et al., 2011, ApJS, 194, 5
Gaia Collaboration et al., 2016a, A&A, 595, A1
Gaia Collaboration et al., 2016b, A&A, 595, A2
Gamen R., et al., 2006, A&A, 460, 777
García B., Malaroda S., Levato H., Morrell N., Grosso M., 1998, PASP, 110, 53
Gardner F. F., Milne D. K., Mezger P. G., Wilson T. L., 1970, A&A, 7, 349
Garmany C. D., Conti P. S., Massey P., 1980, ApJ, 242, 1063
Gieles M., 2013, in Massive Stars: From alpha to Omega. p. 7
Gieles M., Sana H., Portegies Zwart S. F., 2010, MNRAS, 402, 1750
Gies D. R., Bolton C. T., 1986, ApJS, 61, 419
Hénault-Brunet V., et al., 2012, A&A, 546, A73
Herbst W., 1976, ApJ, 208, 923
Hills J. G., 1980, ApJ, 235, 986

Högbom J. A., 1974, A&AS, 15, 417
Huang W., Gies D. R., 2006, ApJ, 648, 580
Huchtmeier W. K., Day G. A., 1975, A&A, 41, 153
Humphreys R. M., 1973, A&AS, 9, 85
Hur H., Sung H., Bessell M. S., 2012, AJ, 143, 41
Iglesias-Marzoa R., López-Morales M., Jesús Arévalo Morales M., 2015, PASP, 127, 567
Kenyon S. J., Hartmann L., 1995, ApJS, 101, 117
Kharchenko N. V., 2001, Kinematika i Fizika Nebesnykh Tel, 17, 409
Kharchenko N. V., Roeser S., 2009, VizieR Online Data Catalog, 1280
Kiminki D. C., Kobulnicky H. A., 2012, ApJ, 751, 4
Kiminki D. C., et al., 2007, ApJ, 664, 1102
Kiminki D. C., et al., 2008, ApJ, 681, 735
Kiminki M. M., Smith N., Reiter M., Bally J., 2017, MNRAS, 468, 2469
Kobulnicky H. A., et al., 2014, ApJS, 213, 34
Kramida A., Ralchenko Y., Reader J., NIST ASD Team 2016, NIST Atomic Spectra Database (version 5.4), http://physics.nist.gov/asd
Kumar B., Sharma S., Manfroid J., Gosset E., Rauw G., Nazé Y., Kesh Yadav R., 2014, A&A, 567, A109
Lada C. J., Lada E. A., 1991, in Janes K., ed., Astronomical Society of the Pacific Conference Series Vol. 13, The Formation and Evolution of Star Clusters. pp 3–22
Lada C. J., Lada E. A., 2003, ARA&A, 41, 57
Levato H., García B., Loustó C., Morrell N., Saizar P., 1986, Rev. Mex. Astron. Astrofis., 13, 3
Levato H., Malaroda S., Garcia B., Morrell N., Solivella G., 1990, ApJS, 72, 323
Levato H., Malaroda S., Morrell N., Garcia B., Hernandez C., 1991a, ApJS, 75, 869
Levato H., Malaroda S., Garcia B., Morrell N., Solivella G., Grosso M., 1991b, Ap&SS, 183, 147
Lindegren L., et al., 2016, A&A, 595, A4
Maíz Apellániz J., et al., 2013, in Massive Stars: From alpha to Omega. p. 198 (arXiv:1306.6417)
Maíz Apellániz J., et al., 2016, ApJS, 224, 4
Markwardt C. B., 2009, in Bohlender D. A., Durand D., Dowler P., eds, Astronomical Society of the Pacific Conference Series Vol. 411, Astronomical Data Analysis Software and Systems XVIII. p. 251 (arXiv:0902.2850)
Martins F., Schaerer D., Hillier D. J., 2005, A&A, 436, 1049
Martins F., Marcolino W., Hillier D. J., Donati J.-F., Bouret J.-C., 2015, A&A, 574, A142
Mason B. D., Hartkopf W. I., Gies D. R., Henry T. J., Helsel J. W., 2009, AJ, 137, 3358
Massey P., 1980, ApJ, 236, 526
Massey P., Conti P. S., 1981, ApJ, 244, 173
Massey P., Johnson J., 1993, AJ, 105, 980
Massey P., Thompson A. B., 1991, AJ, 101, 1408
Massey P., DeGioia-Eastwood K., Waterhouse E., 2001, AJ, 121, 1050
Mayer P., Lorenz R., Drechsel H., Abseim A., 2001, A&A, 366, 558
McClure-Griffiths N. M., Dickey J. M., 2007, ApJ, 671, 427
Megeath S. T., Cox P., Bronfman L., Roelfsema P. R., 1996, A&A, 305, 296
Moe M., Di Stefano R., 2017, ApJS, 230, 15
Moffat A. F. J., 1978, A&A, 68, 41
Moffat A. F. J., Seggewiss W., 1978, A&A, 70, 69
Moffat A. F. J., Seggewiss W., 1979, A&A, 77, 128
Mohr-Smith M., et al., 2017, MNRAS, 465, 1807
Morrell N., Garcia B., Levato H., 1988, PASP, 100, 1431
Morrell N. I., et al., 2001, MNRAS, 326, 85
Morrison N. D., Conti P. S., 1980, ApJ, 239, 212
Munoz M., Moffat A. F. J., Hill G. M., Shenar T., Richardson N. D., Pablo H., St-Louis N., Ramiaramanantsoa T., 2017, MNRAS, 467, 3105
Nazé Y., Antokhin I. I., Sana H., Gosset E., Rauw G., 2005, MNRAS, 359, 688
Niemela V. S., Moffat A. F. J., 1982, ApJ, 259, 213
Niemela V. S., Massey P., Conti P. S., 1980, ApJ, 241, 1050
Niemela V. S., Morrell N. I., Fernández Lajús E., Barbá R., Albacete Colombo J. F., Orellana M., 2006, MNRAS, 367, 1450
Oort J. H., Spitzer Jr. L., 1955, ApJ, 121, 6
Otero S. A., 2006, Open European Journal on Variable Stars, 45, 1
Penny L. R., Gies D. R., Hartkopf W. I., Mason B. D., Turner N. H., 1993, PASP, 105, 588
Pojmanski G., 1997, Acta Astron., 47, 467
Povich M. S., et al., 2011a, ApJS, 194, 6
Povich M. S., et al., 2011b, ApJS, 194, 14
Preibisch T., Mamajek E., 2008, in Reipurth B., ed., , Handbook of Star Forming Regions, Volume II. ASP, San Francisco, CA, p. 235
Preibisch T., Schuller F., Ohlendorf H., Pekruhl S., Menten K. M., Zinnecker H., 2011, A&A, 525, A92
Prša A., Zwitter T., 2005, ApJ, 628, 426
Rathborne J. M., Brooks K. J., Burton M. G., Cohen M., Bontemps S., 2004, A&A, 418, 563
Rauw G., Vreux J.-M., Gosset E., Hutsemekers D., Magain P., Rochowicz K., 1996, A&A, 306, 771
Rauw G., Sana H., Gosset E., Vreux J.-M., Jehin E., Parmentier G., 2000, A&A, 360, 1003
Rauw G., Sana H., Antokhin I. I., Morrell N. I., Niemela V. S., Albacete Colombo J. F., Gosset E., Vreux J.-M., 2001, MNRAS, 326, 1149
Rauw G., Nazé Y., Fernández Lajús E., Lanotte A. A., Solivella G. R., Sana H., Gosset E., 2009, MNRAS, 398, 1582
Rebolledo D., et al., 2016, MNRAS, 456, 2406
Ritchie B. W., Clark J. S., Negueruela I., Crowther P. A., 2009, A&A, 507, 1585
Roberts D. H., Lehar J., Dreher J. W., 1987, AJ, 93, 968
Rochau B., Brandner W., Stolte A., Gennaro M., Gouliermis D., Da Rio N., Dzyurkevich N., Henning T., 2010, ApJ, 716, L90
Rochau B., et al., 2011, MNRAS, 418, 949
Sabín-Sanjulián C., et al., 2014, A&A, 564, A39
Sana H., et al., 2012, Science, 337, 444
Sana H., et al., 2013, A&A, 550, A107
Sana H., et al., 2014, ApJS, 215, 15
Schnurr O., Moffat A. F. J., St-Louis N., Morrell N. I., Guerrero M. A., 2008, MNRAS, 389, 806
Schweickhardt J., Schmutz W., Stahl O., Szeifert T., Wolf B., 1999, A&A, 347, 127
Sexton R. O., Povich M. S., Smith N., Babler B. L., Meade M. R., Rudolph A. L., 2015, MNRAS, 446, 1047
Smith R. G., 1987, MNRAS, 227, 943
Smith N., 2004, MNRAS, 351, L15
Smith N., 2006, MNRAS, 367, 763
Smith N., Brooks K. J., 2007, MNRAS, 379, 1279
Smith N., Brooks K. J., 2008, in Reipurth B., ed., , Handbook of Star Forming Regions, Volume II. ASP, San Francisco, CA, p. 138
Smith N., Conti P. S., 2008, ApJ, 679, 1467
Smith N., Stassun K. G., 2017, AJ, 153, 125
Smith N., Egan M. P., Carey S., Price S. D., Morse J. A., Price P. A., 2000, ApJ, 532, L145
Smith N., Bally J., Brooks K. J., 2004, AJ, 127, 2793
Smith N., Stassun K. G., Bally J., 2005, AJ, 129, 888
Smith N., Bally J., Walborn N. R., 2010a, MNRAS, 405, 1153
Smith N., et al., 2010b, MNRAS, 406, 952
Solivella G. R., Niemela V. S., 1999, in Morrell N. I., Niemela V. S., Barbá R. H., eds, Revista Mexicana de Astronomia y Astrofisica Conference Series Vol. 8, Workshop on Hot Stars in Open Clusters of the Galaxy and the Magellenic Clouds. pp 145–147
Sota A., Maíz Apellániz J., Morrell N. I., Barbá R. H., Walborn N. R., Gamen R. C., Arias J. I., Alfaro E. J., 2014, ApJS, 211, 10
Soubiran C., Jasniewicz G., Chemin L., Crifo F., Udry S., Hestroffer D., Katz D., 2013, A&A, 552, A64
Spitzer L., 1978, Physical processes in the interstellar medium. Wiley-Interscience, New York, NY, doi:10.1002/9783527617722
Steenbrugge K. C., de Bruijne J. H. J., Hoogerwerf R., de Zeeuw P. T., 2003, A&A, 402, 587
Tapia M., Roth M., Marraco H., Ruiz M. T., 1988, MNRAS, 232, 661
Tapia M., Roth M., Vázquez R. A., Feinstein A., 2003, MNRAS, 339, 44
Thackeray A. D., Tritton S. B., Walker E. N., 1973, Mem. RAS, 77, 199

Thé P. S., Vleeming G., 1971, A&A, 14, 120
The P. S., Bakker R., Antalova A., 1980a, A&AS, 41, 93
The P. S., Bakker R., Tjin A Djie H. R. E., 1980b, A&A, 89, 209
Tokovinin A., Fischer D. A., Bonati M., Giguere M. J., Moore P., Schwab C., Spronck J. F. P., Szymkowiak A., 2013, PASP, 125, 1336
Tovmassian H. M., Hovhannessian R. K., Epremian R. A., 1994, Ap&SS, 213, 175
Turner D. G., Moffat A. F. J., 1980, MNRAS, 192, 283
Tutukov A. V., 1978, A&A, 70, 57
Vallée J. P., 2014, AJ, 148, 5
Vazquez R. A., Baume G., Feinstein A., Prado P., 1996, A&AS, 116, 75
Walborn N. R., 1973, ApJ, 179, 517
Walborn N. R., 1982a, AJ, 87, 1300
Walborn N. R., 1982b, ApJ, 254, L15
Walborn N. R., 1995, in Niemela V., Morrell N., Feinstein A., eds, Revista Mexicana de Astronomia y Astrofisica Conference Series Vol. 2, The Eta Carinae Region: A Laboratory of Stellar Evolution. p. 51
Walborn N. R., 2009, in Livio M., Villaver E., eds, Space Telescope Science Institute Symposium Series Vol. 20, Massive Stars: From Pop III and GRBs to the Milky Way. Cambridge University Press, Cambridge, UK, pp 167–177, doi:10.1017/CBO9780511770593.012
Walborn N. R., Hesser J. E., 1975, ApJ, 199, 535
Walborn N. R., Liller M. H., 1977, ApJ, 211, 181
Walborn N. R., et al., 2002a, AJ, 123, 2754
Walborn N. R., Danks A. C., Vieira G., Landsman W. B., 2002b, ApJS, 140, 407
Walborn N. R., Smith N., Howarth I. D., Vieira Kober G., Gull T. R., Morse J. A., 2007, PASP, 119, 156
Walborn N. R., et al., 2014, A&A, 564, A40
Walsh J. R., 1984, A&A, 138, 380
Wang J., et al., 2011, ApJS, 194, 11
Whiteoak J. B. Z., 1994, ApJ, 429, 225
Williams S. J., Gies D. R., Hillwig T. C., McSwain M. V., Huang W., 2011, AJ, 142, 146
Wright N. J., Drew J. E., Mohr-Smith M., 2015, MNRAS, 449, 741
Wright N. J., Bouy H., Drew J. E., Sarro L. M., Bertin E., Cuillandre J.-C., Barrado D., 2016, MNRAS, 460, 2593
Wu Z.-Y., Zhou X., Ma J., Du C.-H., 2009, MNRAS, 399, 2146
Yonekura Y., Asayama S., Kimura K., Ogawa H., Kanai Y., Yamaguchi N., Barnes P. J., Fukui Y., 2005, ApJ, 634, 476
de Bruijne J. H. J., 1999, MNRAS, 310, 585
de Graauw T., Lidholm S., Fitton B., Beckman J., Israel F. P., Nieuwenhuijzen H., Vermue J., 1981, A&A, 102, 257

APPENDIX A: PERIODOGRAMS

Here we present frequency power spectra for the binary systems fit in Section 3. We use the discrete Fourier transform (DFT) and one-dimensional `CLEAN` algorithm[4] of Roberts et al. (1987) as implemented in IDL by A. W. Fullerton (see Fullerton et al. 1997). The DFT is computed up to a maximum frequency of $f_{\rm max} = 1/(2\Delta t_{\rm min})$, where $\Delta t_{\rm min}$ is the minimum time interval between observations. `CLEAN` deconvolves the window function from the DFT, removing aliases introduced by uneven time sampling. We run `CLEAN` for 100 iterations with a gain of 0.5.

The resulting periodograms are used first to check for periodicity and second to corroborate the periods found by the orbital fitting package `rvfit` (Iglesias-Marzoa et al. 2015) for HD 92607, HD 93576, and HDE 305536. `rvfit` does not require an intial estimate of the period, and we leave the period as a free parameter when fitting these three systems. For the eclipsing binary HDE 303312, we fix the period in `rvfit` at the photometric period as described in Section 3.3.

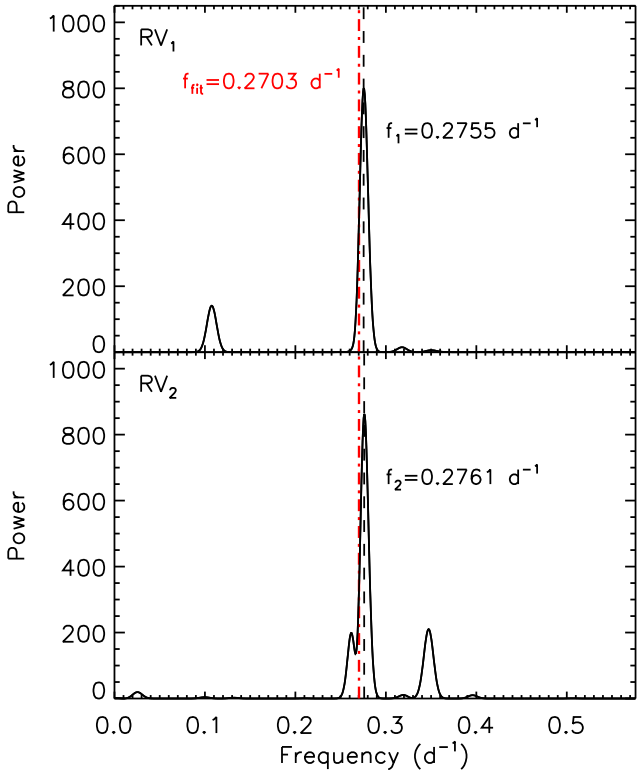

Figure A1. `CLEAN`ed power spectra of the primary (top) and secondary (bottom) RV components of the SB2 HD 92607. The black dashed lines mark the frequencies f_1 and f_2 corresponding to the strongest peak in each power spectrum. The red dot-dash line in both panels indicates the frequency $f_{\rm fit}$ corresponding to the final best-fitting orbital period from an unconstrained simultaneous fit to both components with `rvfit`.

The periodograms for the primary and secondary components of HD 92607 (Figure A1) both have clear peaks at frequencies of ≈ 0.276 d^{-1}, corresponding to a period of ~ 3.6 d. The full, unconstrained fit with `rvfit` (see Section 3.1) finds a period of 3.6993 d. Visual inspection of phase-folded RV curves rules out most common possible alias periods. We cannot definitively exclude the $1 + f$ alias, which is above our maximum searchable frequency and corresponds to a period of ~ 0.79 d; however, a sub-day period would be extremely unusual for a main-sequence O+O binary (Kiminki & Kobulnicky 2012; Sana et al. 2012; Moe & Di Stefano 2017; Almeida et al. 2017).

The components of HD 92607 are of very similar spectral type (O8.5 V + O9 V; Sexton et al. 2015). If we swap the values of RV$_1$ and RV$_2$ at several epochs, the periodograms of both components show clear peaks at 0.538 d^{-1}, or a period of 1.859 d. With these component assignments, `rvfit` finds a plausible solution for a similar period of 1.84957 d. This fit requires a substantial eccentricity ($e = 0.35$) and an approximate inclination of 45°.

The periodogram derived from our CHIRON data for HD 93576 (upper panel in Figure A2) shows a single strong peak at a frequency of 0.543 d^{-1}, or a period of 1.84 d. A similar peak appears when this system's data from Levato et al. (1990) are included (lower panel of Figure A2). The full, unconstrained fit with `rvfit` to the combined data set (see Section 3.2) finds a period of 1.852102 d. Before `CLEAN`ing, the DFT for HD 93576 also shows a

[4] The two-dimensional `CLEAN` algorithm was first developed by Högbom (1974).

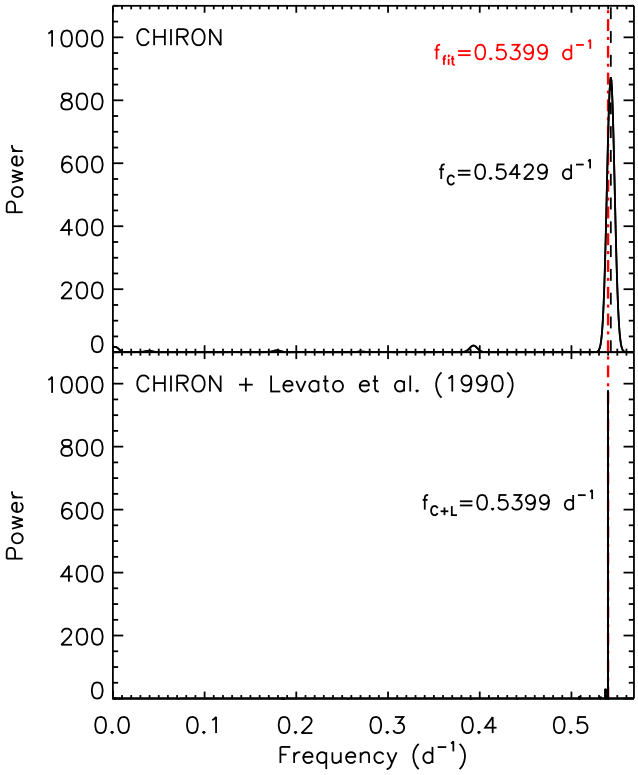

Figure A2. Top: CLEANed power spectrum of our CHIRON RV data for the SB1 HD 93576. The black dashed line marks the frequency f_C corresponding to the strongest peak. Bottom: as above, including RV data from Levato et al. (1990). The frequency f_{C+L} corresponds to the strongest peak. The red dot-dash line in both panels indicates the frequency f_{fit} corresponding to the final best-fitting orbital period from an unconstrained fit to the combined data set with `rvfit`.

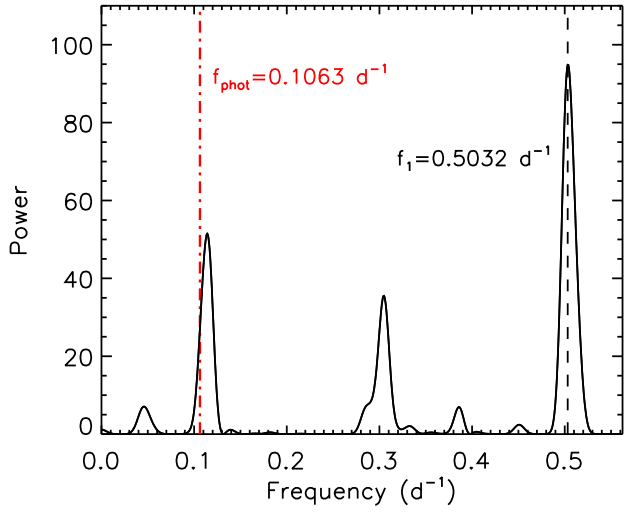

Figure A3. CLEANed power spectrum of our CHIRON RV data for the eclipsing SB1 HDE 303312. The black dashed line marks the frequency f_1 corresponding to the strongest peak. The red dot-dash line indicates the frequency f_{phot} of the ASAS V-band light curve.

peak at the $1 - f$ alias of 0.460 d^{-1}, or a period of 2.174 d. We can force a plausible solution at this period in `rvfit` if we constrain the range of allowed periods and fit only to our CHIRON data; the combined data set including Levato et al. (1990) RVs is incompatible with this period. As this alias peak is removed by the CLEAN deconvolution, it appears to be an artifact of our observational time sampling.

The RV periodogram for the eclipsing binary HDE 303312 (Figure A3) has several peaks. The strongest peak is at a frequency of 0.503 d^{-1} or a period of 1.99 d. This period—which, as a near-integer multiple of days, is likely a sampling artifact—is ruled out by visual inspection of the phase-folded RV curve and by constrained tests in `rvfit`. The second-highest peak in the periodogram is at a frequency of 0.114 d^{-1}, or a period of ~ 8.8 d. Unconstrained fits in `rvfit` converge on a period between 9.41 and 9.65 d, close to the photometric period of 9.4111 d (which corresponds to a frequency of 0.10626 d^{-1}). As described in Section 3.3, we fix the period at the photometric period for subsequent fitting.

The periodogram derived from our CHIRON data for HDE 305536 (top panel of Figure A4) has its highest peak at a frequency of 0.526 d^{-1} or a period of 1.90 d. A similar peak frequency is found when this system's data from Levato et al. (1990) are included (bottom panel of Figure A4). Visual inspection of phase-folded RV curves and constrained tests in `rvfit` rule out common possible aliases. The full, unconstrained fit to our CHIRON data with `rvfit` finds an orbital period of 1.88535 d, corresponding to

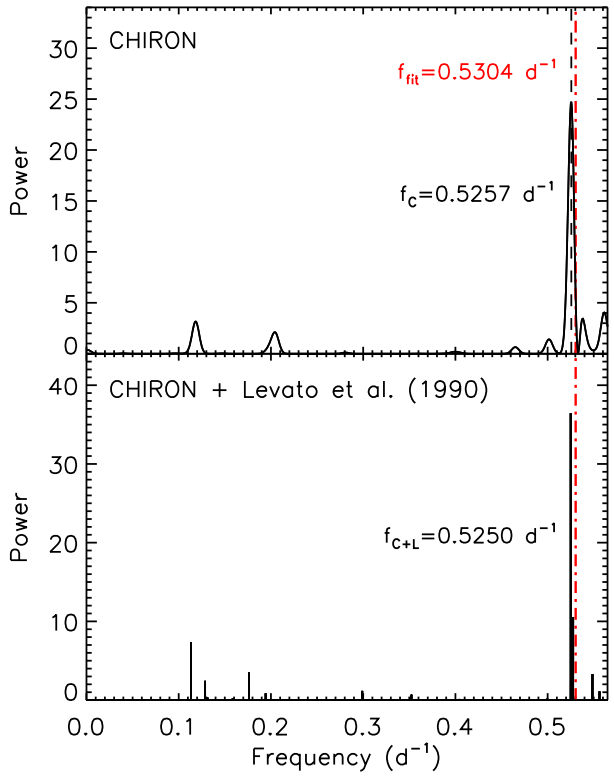

Figure A4. Top: CLEANed power spectrum of our CHIRON RV data for the SB1 HDE 305536. The black dashed line marks the frequency f_C corresponding to the strongest peak. Bottom: as above, including RV data from Levato et al. (1990). The frequency f_{C+L} corresponds to the strongest peak. The red dot-dash line in both panels indicates the frequency f_{fit} corresponding to the final best-fitting orbital period from an unconstrained fit to our CHIRON data with `rvfit`.

a frequency of 0.53041 d^{-1}. As described in Section 3.4, `rvfit` is unable to converge on a solution that includes the Levato et al. (1990) data.

This paper has been typeset from a TEX/LATEX file prepared by the author.